

ACKNOWLEDGEMENTS AND DECICATIONS

To God, I thank for giving me the amazing opportunity of being involved in this project, for all the people surrounding me who have touched my life and supported me in this journey, and for strength and motivation that I needed to produce this presented work that fills me with pride. This thesis is dedicated to Dr. Ronald J. Doll, whose patience and dedication guided me through the completion of such an ambitious project and who has been a constant source of knowledge and inspiration to me. La perseverancia que he puesto en esta investigación se lo dedico a mis padres, Verushka Maurera y Germán Sánchez, quienes forjaron en mí la dedicación y empuje que se requerían para un proyecto como este y quienes han hecho posible el cumplimiento de mis sueños. A mi hermano, Germán I. Sánchez, quien me inspira cada día a ser una mejor científica, hermana y mujer, le dedico el esfuerzo que he puesto para avanzar en el camino hacia la cura del cáncer – gracias a ti tuve las fuerzas de ir al laboratorio con una sonrisa todos los días.

I would also like to thank **Drew University**, specifically the **Research Institute for Scientist Emeritus (RISE) and Chemistry Departments, and the Drew Summer Science Institute (DSSI)**, with special acknowledgements to Dr. Bimal Dasmahapatra, Dr. C. Anderson Evans, and my committee members Dr. Christopher Andrews and Dr. Mary-Ann Pearsall. I would like to give a special recognition to the previous students that worked on this project and helped me embark in this research, Megan McAlavy and Joshua Hsu.

Sin Dios, la Virgen, y mi familia, este trabajo no hubiese sido posible.

Drew University
College of Liberal Arts

**Evaluation of Human Liver Metabolism of Compounds that
Reactivate Mutant p53 in Human Cancer Cells**

An Honors Thesis in Chemistry
By: Stephanie C. Sánchez

Submitted in partial fulfillment
Of the Requirements
For the degree of
Bachelor in Arts
With Specialized Honors in Chemistry

April 2016

ABSTRACT

A recent approach for a cancer therapy is the reactivation of the mutant p53, tumor suppressor protein that is mutated in about 50% of all human cancers. The Doll Lab has identified compounds of the benzimidazole class that reactivate mutant p53 in human cancer cells. Drug discovery is concerned with the optimization of lead structures that show biological activity towards targeted diseases. This involves optimization of compounds that have improved potency, selectivity and drug-like properties. Two critical drug-like properties are the ability of a compound to cross biological membranes and to possess human metabolic stability. Metabolic stability is important for patient compliance and lower dose/toxicity of compounds. Thus, as part of the optimization of such lead structures, the metabolic profile has to be evaluated – which in this context includes metabolic rate and the identity of metabolites. This research focuses on improving metabolic profiles of candidate drugs by establishing a structural activity relationship for the *in vitro* human metabolism. We determined the benzimidazole class of compounds undergo hydroxylation by CYP450 in the Phase I metabolism by human liver microsomes. In order to improve metabolic stability, structural changes were made to the lead benzimidazole compounds. We report here that addition of electron-withdrawing groups – like fluorine – to the benzimidazole ring portion of the lead structures slowed down the metabolic rate. Furthermore, addition of electron-donating groups – such as methyl – to the benzimidazole ring portion accelerated the metabolic rate by CYP450. All synthesized and studied compounds undergo at least single hydroxylation by CYP450 at the benzimidazole ring portion. Amide benzimidazole analogues were found to be less metabolically stable than urea benzimidazole analogues prior to fluorination. Once fluorinated, amide and urea benzimidazoles were closer in metabolic rates – which indicates that the effect of fluorination on amide benzimidazoles is larger than in urea benzimidazoles. We find the fluorinated benzimidazole analogues have metabolic rates that are similar to metabolic rates of some marketed drugs. This indicates the benzimidazole class of compounds is a reasonable structural class for drug discovery. Newly synthesized compounds still have to be evaluated for membrane transport rate for the GI and BBB membranes, as well as the reactivation of mutant p53 and toxicity in human cancer cells.

TABLE OF CONTENTS

	Page
INTRODUCTION.....	4
<i>Cancer.....</i>	4
<i>The Drug Discovery Process.....</i>	4
<i>Mutant p53 Reactivation: An Oncology Project.....</i>	6
<i>p53 and Cancer.....</i>	7
<i>Compounds that Reactivate Mutant p53.....</i>	12
<i>ADME Pharmacokinetics: Improving Metabolic Rates.....</i>	13
<i>Human Liver Metabolism: Cytochrome P450.....</i>	15
<i>In vitro Human Metabolism: Microsomes.....</i>	18
<i>Modification of Metabolic Rates.....</i>	20
RESEARCH OBJECTIVE.....	24
EXPERIMENTAL SECTION.....	27
<i>Synthetic Strategies.....</i>	27
<i>Mechanism of Synthetic Strategies.....</i>	28
<i>Reagents.....</i>	29
<i>Characterization.....</i>	29
<i>Synthetic Pathways.....</i>	30
<i>Synthesis of Intermediates.....</i>	30
<i>Fluoro-Intermediate.....</i>	30
<i>Methyl-Intermediate.....</i>	32
<i>Synthesis of Amides.....</i>	35
<i>Amide-F (RD 78).....</i>	35
<i>Synthesis of Ureas.....</i>	37
<i>Urea-F (RD 86).....</i>	37
<i>Urea-M (RD 89).....</i>	40
<i>Biological Evaluation of the p53 Reactivation Process.....</i>	42
<i>Phase I In vitro Metabolism.....</i>	43
<i>Solutions.....</i>	43
<i>Procedure.....</i>	44
<i>Treatment of Each Aliquot.....</i>	44
<i>Compound Concentration Calculation.....</i>	44
<i>Identification of Metabolites.....</i>	45
<i>Metabolic Rate and Intrinsic Clearance Calculations.....</i>	47
RESULTS.....	52
<i>Metabolic Rates and Intrinsic Clearance.....</i>	52
<i>Determination of Metabolites.....</i>	55
DISCUSSION.....	65
<i>Metabolism of RD compounds.....</i>	66
<i>Metabolic Data.....</i>	71
<i>Amide versus Ureas.....</i>	71
<i>Fluorinated Compounds versus Non-Fluorinated Compounds.....</i>	73
<i>Fluorination of Amides versus Fluorination of Ureas.....</i>	74

<i>Effects of Electron-donating Group</i>	74
<i>LogP, CLogP, and Lipophilicity</i>	75
<i>Intrinsic Clearance Category</i>	77
<i>Marketed Drugs</i>	78
CONCLUSION	81
<i>Future considerations</i>	82
<i>References</i>	84

TABLE OF FIGURES

FIGURE	Page
FIGURE 1: Examples of Hallmarks of Cancer and p53 Response.....	7
FIGURE 2: X-Ray Crystal Structure of p53.....	8
FIGURE 3: p53 Pathway.....	10
FIGURE 4: Conformations of p53.....	11
FIGURE 5: Compounds that Reactivate Mutant p53.....	12
FIGURE 6: Phase I and II Metabolisms in the Liver.....	16
FIGURE 7: CYP450 Cycle.....	17
FIGURE 8: Structural Modification of a Drug.....	21
FIGURE 9: Lead Structures in Doll's Lab.....	22
FIGURE 10: Benzimidazole.....	25
FIGURE 11: Liquid Chromatogram for F-Intermediate.....	31
FIGURE 12: Mass Spectrum for F-Intermediate.....	31
FIGURE 13: NMR Spectrum for F-Intermediate.....	32
FIGURE 14: Possible Tautomers for M-Intermediate.....	33
FIGURE 15: Liquid Chromatogram for M-Intermediate.....	33
FIGURE 16: Mass Spectrum for M-Intermediate.....	34
FIGURE 17: NMR Spectrum for M-Intermediate.....	34
FIGURE 18: Liquid Chromatogram for Amide-F.....	36
FIGURE 19: Mass Spectrum for Amide-F.....	36
FIGURE 20: NMR Spectrum for Amide-F.....	37
FIGURE 21: Liquid Chromatogram for Urea-F.....	38
FIGURE 22: Mass Spectrum for Urea-F.....	39
FIGURE 23: NMR Spectrum for Urea-F.....	39
FIGURE 24: Liquid Chromatogram for Urea-M.....	40
FIGURE 25: Mass Spectrum for Urea-M.....	41
FIGURE 26: NMR Spectrum for Urea-M.....	41
FIGURE 27: TIC Chromatogram for Amide-H.....	46
FIGURE 28: Extracted Ion Chromatogram for Amide-H Metabolite 1.....	46
FIGURE 29: Extracted Ion Chromatogram for Amide-H Metabolite 2 and 3.....	47
FIGURE 30: Metabolic Data on Excel.....	48
FIGURE 31: Inserting Metabolic Graph on Excel.....	49
FIGURE 32: Metabolic Graph on Excel.....	49
FIGURE 33: Inserting Label on Metabolic Graph.....	50
FIGURE 34: Linear Trendline on Excel.....	51
FIGURE 35: Urea-H Metabolic Rate.....	52
FIGURE 36: Amide-H Metabolic Rate.....	53
FIGURE 35: Amide-F Metabolic Rate.....	53
FIGURE 38: Urea-F Metabolic Rate.....	54
FIGURE 39: Urea-M Metabolic Rate.....	54
FIGURE 40: LC for Amide-H Microsomal Assay.....	55
FIGURE 41: MS for Amide-H Microsomal Assay.....	56

FIGURE 42: LC for Amide-F Microsomal Assay.....	57
FIGURE 43: MS for Amide-F Microsomal Assay.....	58
FIGURE 44: LC for Urea-H Microsomal Assay.....	59
FIGURE 45: MS for Urea-H Microsomal Assay.....	60
FIGURE 46: LC for Urea-F Microsomal Assay.....	61
FIGURE 47: MS for Urea-F Microsomal Assay.....	62
FIGURE 48: LC for Urea-M Microsomal Assay.....	63
FIGURE 49: MS for Urea-M Microsomal Assay.....	64
FIGURE 50: Metabolic Rates for Targeted Compounds.....	65
FIGURE 51: Urea-H Metabolite.....	67
FIGURE 52: Amide-H Metabolite.....	68
FIGURE 53: Amide-F Metabolite.....	68
FIGURE 54: Urea-F Metabolite.....	69
FIGURE 55: Urea-M Metabolite.....	70
FIGURE 56: Fragmentation under MS Conditions.....	72
FIGURE 57: Hetero-Bond Cleavage under MS Conditions.....	73
FIGURE 58: Possible Sites of Hydroxylation for Urea-H.....	75
FIGURE 59: Distribution of CLogP for Marketed Drugs.....	77
FIGURE 60: Comparison of <i>In vitro</i> Data with Marketed Drugs.....	7

GLOSSARY

ADME: absorption distribution metabolism excretion of a compound

Angiogenesis: development of new blood vessels

Apoptosis: process of programmed cell death

BAX: BCL2-associated X protein involved in apoptosis

BBB: blood brain barrier. Blood vessel membranes that separates the CNS from the systemic circulation

Cancer: group of diseases involving abnormal cell growth and invasion into other tissues

Cell: basic structural, functional, and biological unit of living organisms

Chromatogram: a visible record showing the results of separation of the components of a mixture by chromatography

Clearance: pharmacokinetic measurement of the volume of plasma that is completely cleared off of a substance per unit of time

CLogP: calculated Log P

CNS: Central Nervous System.

Cofactor: substance whose presence is essential for activity of an enzyme

CYP: cytochrome p450; drug metabolizing enzyme that causes free radical hydroxylation of substrates. Also denoted as P450 or CYP450.

DMSO: Dimethyl sulfoxide solvent

Drug-Like Property: qualitative properties a compound should have to be a potential drug. These properties include: metabolic stability, membrane permeability, absorption, amongst others.

Gene: region of DNA that encodes protein products

Endogenous: originating within an organism

Enzyme: biological molecule that acts as catalyst and helps complex reactions to occur

Hydroxylation: chemical process that introduces a hydroxyl group into an organic compound

In vivo: studies in which the effects of biological entities are tested on whole, living organisms

In vitro: studies in which the effects of biological entities are tested on partial or dead organisms

Intrinsic Clearance: ability of the liver to remove drug in the absence of flow limitations and binding to cells or proteins in the blood. Intrinsic clearance is the intrinsic capacity of liver microsomes to metabolize a drug by phase I metabolism

Isoenzyme: enzymes that differ in the amino acid sequence but catalyze the same chemical reaction

LC/MS: Liquid Chromatography coupled with Mass Spectrometry

LogP: partition coefficient (solubility) of a compound between water and n-octanol

MDM2: Mouse double minute 2 homolog. Enzyme responsible for degrading p53.

Metabolism: chemical reactions involved in maintaining the living state of the cells and the organism

Metabolite: substance formed in or necessary for metabolism

MS: Mass Spectrometry

MW: Molecular weight

MW+1: Molecular weight plus 1 (addition of H atom) in the Mass Spectrometer

NADPH: nicotinamide adenine dinucleotide phosphate

NMR: Nuclear magnetic resonance

Null Cells: Cells lacking a specific gene or protein

Oncogene: a gene that in certain circumstances can transform a cell into a tumor cell

Pharmacokinetics: describes the rate of Absorption, Distribution, Metabolism, and Excretion (ADME)

Pharmacokinetic profile: The profile that describes the ADME properties of a molecule

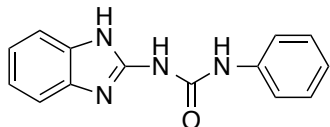
p53: A tumor-suppressor protein that functions as a transcription factor for many cell control proteins

Protein: large biomolecule consisting of one or more chains of amino acid residues

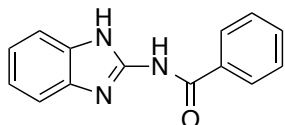
PUMA: BCL-2-binding component 3

RD #: Sequential number of compound synthesized in Dr. Doll's lab (RISE)

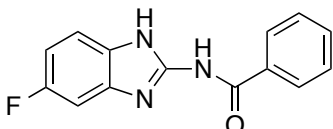
RD 38: Urea-H. Un-substituted urea benzimidazole.



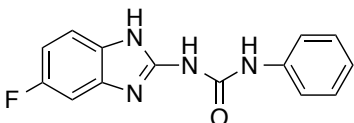
RD 53: Amide-H. Un-substituted amide benzimidazole.



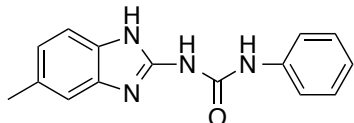
RD 78: Amide-F. Fluorinated amide benzimidazole.



RD 86: Urea-F. Fluorinated urea benzimidazole.



RD 89: Urea-M. Methyl urea benzimidazole.



SAR: Structure activity relationship of a class of compounds

Substrate: material upon which an enzyme acts

TI: Therapeutic Index. This is the ratio between the amount of drug that causes therapeutic effect to the amount that causes toxicity.

TIC: Total ion current. It represents the summed intensity across the entire range of ion masses being detected at every point in the analysis by LC/MS.

TOF: Time of flight mass spectrometer. Method of mass spectrometry by which an ion mass-to-charge ratio is determined via a time measurement.

Tumor: abnormal mass of tissue

T_{1/2}: amount of time required for the concentration of drug to fall to half its initial value.

Wild-type: protein which is free of mutations in the biological system.

INTRODUCTION

Cancer

Cancer is the general name of a wide range of diseases, which have two important characteristics in common: uncontrolled growth of abnormal cells and the ability of cancer cells to cross membranes and grow in different tissue areas. Currently, cancer is the second leading cause of death in the United States (American Cancer Society, 2015). According to the incidence and mortality data for the United States from 2009 through 2011 (most recent years available) provided by the U.S. National Cancer Institute's Surveillance Epidemiology and End Results (SEER), the risk of developing cancer is 43.31% and 37.81%, for men and women respectively, and the risk of dying from it is 22.83% and 19.26% for males and females, respectively. With the increasing risk of developing any variation of cancer, it is relevant for the scientific community to engage in the development of more effective cancer therapies.

The Drug Discovery Process

Since 1856, when William Perkin synthesized mauveine in London, chemists and medicinal chemists have been working on synthetic drugs in laboratories across the world (Sneader, 2005). Synthetic drugs allow researchers to design and synthesize new compounds that show improved biological activity towards a targeted disease. This medicinal chemistry methodology opens the possibility of developing compounds that can lead to novel or improved therapies.

Drug discovery is the process by which chemical compounds are identified and developed into new possible medications (Sneader, 2005). It involves the identification of compounds that have therapeutic effects on the specific targeted disease. The initial compounds that show biochemical activity are called lead compounds (Sneader, 2005). Medicinal chemists then optimize the lead compounds into a compound with the best possible potency, selectivity and drug like properties. This optimized compound then becomes a candidate for *in vivo* studies to test for efficacy and toxicity. If efficacy and toxicity are suitable, the compound can enter clinical trials in humans. This process is outlined below (Mizuno, 2003).

Drug Discovery Process	
1	Identification, validation, and development of assays for the biological target relevant to a disease state.
2	Screening and identification of lead structures.
3	Optimization of lead structures to increase potency and selectivity.
4	Optimization of lead structures to improve <i>in vitro</i> drug-like properties.
5	<i>In vivo</i> studies to test for efficacy and low toxicity.
6	Clinical trials in humans with best compounds.

Table 1. Simplified summary of the drug discovery process.

The goal of any drug discovery project is to optimize the potential drug compounds for potency, selectivity, and drug-like properties by following a structure activity relationship (SAR) of the synthesized compounds. This developing SAR should set the guidelines in designing new compounds to synthesize. Potency is a measure of how well the compounds work at modulating the activity of a specific target, and selectivity is a measure of how the specific target is modulated versus other targets

(Walker, 2006). Drug-like properties describe many physical and chemical properties found in marketed drugs; for example, solubility, bioavailability, metabolic stability, and membrane permeability, amongst others.

The optimum metabolic profile of a drug is critical to assure the correct drug exposure in a patient at a given dose. The overall profile of a compound's absorption, metabolism and excretion is referred as the pharmacokinetic profile.

Mutant p53 Reactivation: An Oncology Project

Since cancer is an arrangement of complex diseases, a single "cure" for cancer does not exist in the current world of medicine (Enger, 2007). Some of the current therapies used to treat cancer are listed in **Table 2**.

	Current Cancer Therapy
1	Surgery
2	Radiation Therapy
3	Cytotoxic Chemotherapy
4	Target directed Therapy (small molecule or biological)

Table 2. A list of current cancer therapies used to treat the disease according to the stage and location of the tumor. Surgery is performed when the tumor is accessible and its removal will not cause collateral damage (Subotic, 2012). Radiation therapy is performed by using ionizing radiation to kill cancer cells and shrink the tumor (Takimoto, 2008). Cytotoxic chemotherapy utilizes drugs such as taxol and cis-platinum to affect dying cells in general (Takimoto, 2008). Finally, target directed therapy aims for inhibition of specific onco-pro-tumor agents (Duarte, 2009).

However, as cancer rises to the second leading cause of death in the United States, it becomes imperative to find alternative therapies that show better efficacy and less

toxicity. One such attempt that has been investigated since 2003 is the reactivation of mutant p53 as a potential novel anti-cancer therapy approach (Wiman, 2010).

There are currently ten hallmarks of cancer, **Figure 1** shows three examples of hallmarks and how p53 – a critical protein involved in cancer targeting – responds to these events in the cell.

Hallmark	p53 Response
Activating Invasion and Metastasis	Expresses p21, which Causes Cell Cycle Arrest
Resisting Cell Death	Expresses BAX and PUMA, which Induce Apoptosis
Inducing Angiogenesis	Expresses BAI1 and Maspin, which Inhibit Angiogenesis

Figure 1. Three examples of hallmarks of cancer and how protein p53 responds to these events in the cell.

p53 and cancer

In 1979, the p53 gene was the first tumor-suppressor gene to be identified (Bullock, 2001); it was originally thought to be an oncogene – which is a gene with the potential to cause cancer – but functional data showed it to be a tumor suppressor. When p53 is activated, it binds to DNA as a tetramer as shown in **Figure 2**. This complex acts as a transcription factor for many cell proteins that control cell growth and viability (Volgstein, 2000). The p53 tumor suppressor protein acts as a stop sign to the cell cycle and DNA replication when cells are stressed or damaged. Mutations of the p53 protein

can prevent it from performing its function as a tumor suppressor, leading to uncontrolled growth of abnormal cells, which is one of the hallmarks of cancer (Volgstein, 2000).

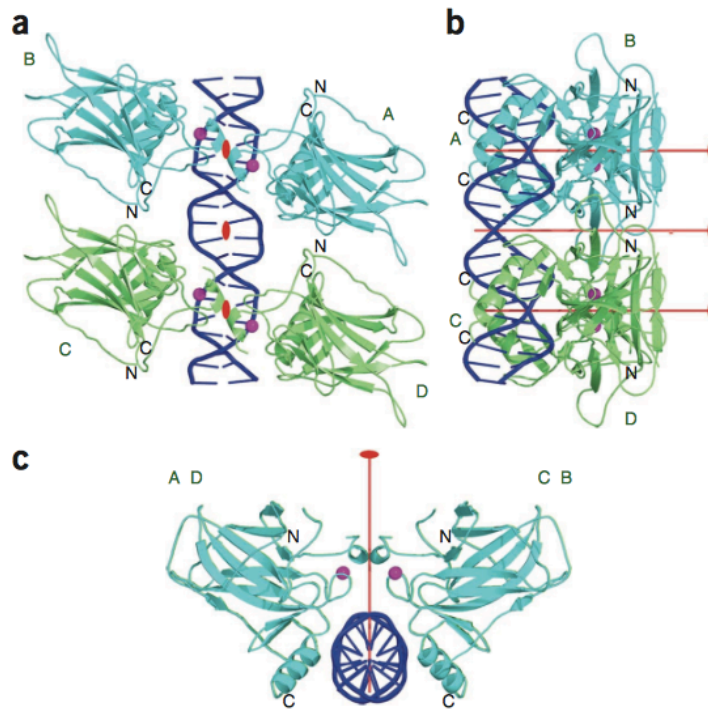


Figure 2. X-ray crystal structure of the tumor suppressor protein p53 bound to DNA as a tetramer. Only the binding domains for p53 are depicted since the crystal structure of the rest of the protein is not known due to its lack of stability. The dark blue structure represents DNA (Kitayner, 2010). Three different views are shown for the bound protein to DNA: **a)** front view, **b)** side view, and **c)** top view.

Figure 3 describes the activation pathway of wild type p53 in human cells. The p53 activation pathway begins by inhibiting the activity of MDM2, a negative p53 regulator. The p53 activation could arise by even a single break in a double-stranded DNA (Volgstein, 2000). This implies that the p53 protein pathway is very sensitive. Overall, there are three pathways that could cause stress or damage to the cell (Volgstein, 2000). The first cause is indeed DNA damage – such as the one caused by

ionizing radiation. A second factor is aberrant growth signals. Finally, a third pathway is induced by a wide range of chemotherapeutic drugs, ultraviolet light, and protein-kinase inhibitors. All of these three pathways activate p53 by inhibiting the degradation of p53 (Volgestein, 2000). Increased concentrations of activated p53 allow it to bind to DNA and activate various gene expressions. These expressed proteins, such as p21, ultimately lead – directly or indirectly – to inhibition of cell division or cause apoptosis (Volgestein, 2000). When the p53 gene is mutated, the resulting mutated p53 protein fails to express the required cell control proteins, allowing damaged or stressed cells to replicate, forming tumors. This offers an explanation for why the inactivated, mutated, p53 protein is so often found in human cancers (Volgestein, 2000). When p53 is mutated, cells containing oncogenic mutations continue to proliferate, resulting in cancer (Chen, 1990). The mutations on p53 common mutations are in the DNA binding domain and mostly are at six following positions on p53 – Arg-248, Arg-273, Arg-175, Gly-245, Arg-249, Arg-282 (Joerger, 2006). These point mutations are located in the DNA binding domain, causing a conformational shift in p53, leading to the inability of p53 to bind to DNA, a necessary step for p53 to activate the expression of downstream proteins.

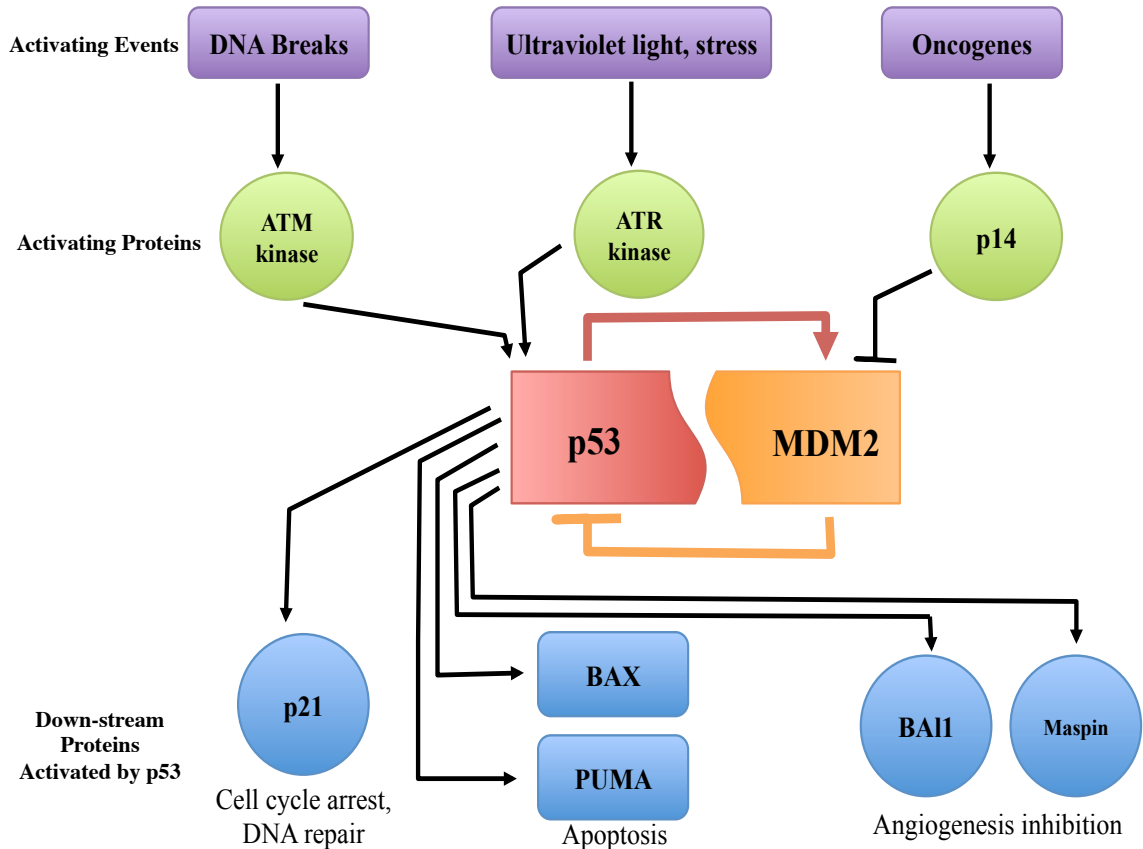


Figure 3. Wild type p53 is activated when cells are stressed, when an oncogene is identified, or when DNA is damaged. Shutting down the replication of such cells by inhibiting the progress of the cell cycle is critical (Volgestein, 2000). When these factors are perceived, p53 is activated and the MDM2 complex is dissembled by phosphorylation of MDM2. MDM2 catalyzes the degradation of p53 when it is no longer needed. Activated p53 binds to DNA and acts as a transcription factor; p53 stimulates the expression of p21, which is an inhibitor of cyclin-dependent kinases (CDKs). CDKs are key regulators to cell cycle (Volgestein, 2000). This allows DNA repair mechanisms to take place, or cell death if the DNA cannot be repaired.

In 1989, it was found that p53 is mutated in approximately 50% of all human cancers (Hoe, 2014). Mutant p53 is no longer capable of acting as a tumor suppressor; furthermore, mutant p53 can inhibit wild-type p53 protein target gene transcription and tumor suppressor function, which can accelerate cancer progression and increases tumor invasiveness (Goh, 2011). Recent studies have shown that small-molecules can bind to

mutant p53 and restore its biological activity as a tumor suppressor. Such a drug might offer a novel anti-cancer therapy (Bullock, 2001). This is achievable because, as depicted in **Figure 4**, both wild type and mutant p53 are in equilibrium with an active and inactive conformation. In mutant p53, the equilibrium predominantly favors the inactive conformation of the protein. Small molecules have been found that shift the equilibrium towards the active conformation, thus reactivating the mutant p53. The drug-p53 complex can then enter the nucleus and bind to DNA, thus displacing the drug. The p53-DNA complex should then act as a wild type p53-DNA complex, thus restoring the activity of mutant p53. The viable approach is to find small organic molecules that can change the conformation of mutant p53, allowing it to bind to DNA and cause transcription of p21 and other downstream proteins (Bullock, 2001). Of course, the reactivated p53 may not induce the transcription of every downstream protein as wild type p53 does, and not every p53 mutant form may be reactivated by the same drug.

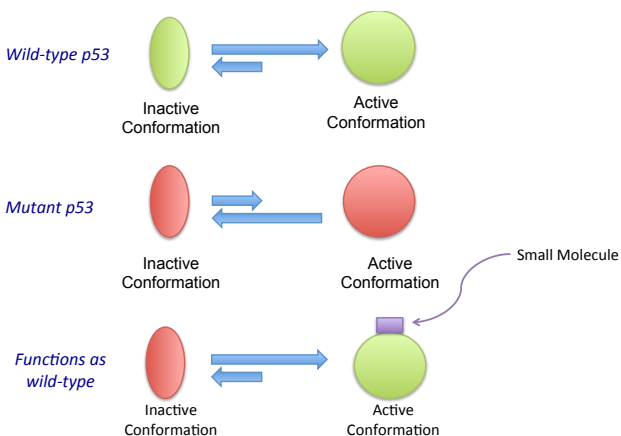


Figure 4. Conformations of p53, showing the chemical equilibrium between the active and inactive conformations of the protein. Green p53 represents wild-type protein, red p53 represents mutated protein, and it is shown how binding of a small molecule will shift the equilibrium towards the activate conformation, restoring activity of wild-type p53.

Compounds that Reactivate Mutant p53

Thus, the goal is to design mutant p53 reactivation compounds that are potent, selective, and have drug like properties. Recently, researchers have identified compounds that can reactivate mutant p53 (Bullock, 2001). **Figure 5** shows the two examples that inspired this project in the search for small organic molecules that could bind to and reactivate mutant p53 in human cancer cells.

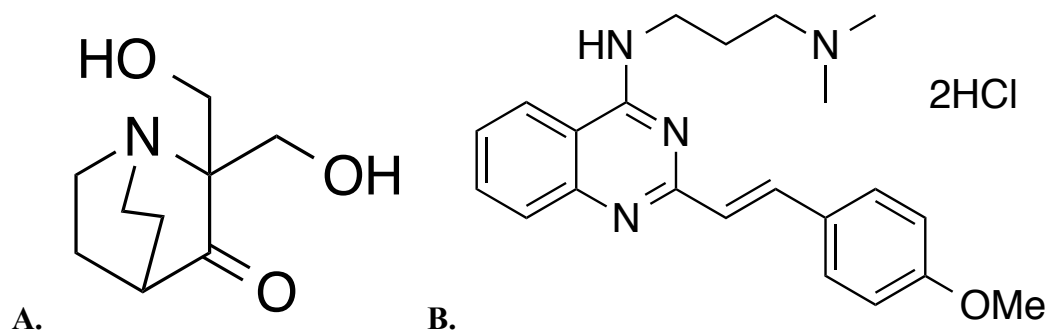


Figure 5. **A.** Structure of Prima 1, a compound that was found to bind to and reactivate mutant p53 in human cancer cells. **B.** Structure of CP-31398, a compound found to bind to and reactivate mutant p53.

One example of a small organic molecule that binds to and reactivates mutant p53 is Prima-1, a compound that is in clinical trials reported to reactivate mutant p53 in human cancer cells (Wiman, 2010). However, this compound was later shown to be also working by mechanisms other than just binding to mutant p53 (Cui, 2014), including forming covalent bonds with mutant p53 as well as causing apoptosis in p53 null cells (Lambert, 2009). This means that Prima-1 could cause general toxicity to the cells, making it a poor drug for the treatment of cancers with mutant p53. Clinical trials for Prima-1 are still ongoing.

Another compound, CP-31398, provided very promising results in its ability to

induce apoptosis in cancer cells with mutant p53 (Takimoto, 2002). However, the compound was highly toxic to healthy cells due to its ability to also bind to DNA (Wang, 2003). In a review published in 2003, it was suggested that small organic compounds that reactivate mutant p53 would be very advantageous and effective if they were potent, selective, and had drug-like properties (Bykov, 2003).

Both CP-31398 and Prima-1 can restore p53-dependant transcription activity of mutant p53 (Brown, 2006). Thus, compounds that stabilize mutant p53 in the active form constitute a promising drug discovery and therapeutic approach to reactivate p53 transcriptional activity in human cancer cells.

High throughput screening (biological testing of many compounds in a short period using robotics) is a widely used technique currently implemented in the pharmaceutical industry to identify compounds that potentially have biological activity towards a specific targeted disease. This technique has identified compounds that stabilize mutant p53 and unfold it into a wild-type p53 (Brown, 2006).

ADME Pharmacokinetics: Improving Metabolic Rates

Pharmacokinetics describes the process of Absorption, Distribution, Metabolism, and Excretion (ADME) of a compound when administered to a living animal (Ruiz-Garcia, 2008). The absorption of the drug can be predicted by the transport rate of crossing the biological membranes in the gastrointestinal (GI) track (Mosby, 2006), (Knights, 2002). After crossing the intestinal GI membranes, the compound enters the portal vein and goes directly to the liver, where first-pass metabolism takes place (Ruiz-Garcia, 2008). The remaining compound and metabolites then enter the general

circulatory system where the compounds are distributed throughout the body (Ruiz-Garcia, 2008). Metabolites and parent drug can have biological effects. The compounds in the circulatory system eventually reenter the liver for additional metabolism. Eventually, all metabolites and un-metabolized parent drugs are excreted (i.e., cleared). This is a continuous process, and the longer the parent drug remains in the system, the greater the biological effects (Knights, 2002). The purpose of the metabolism of a drug is to increase the polarity, or water solubility, of a drug, so the metabolites can be excreted by the kidney or through the bile easily.

The human liver metabolism of drugs can be followed in the laboratory by performing *in vitro* studies using human liver microsomes. The goals of studying the *in vitro* metabolic profiles are to improve the intrinsic clearance (measured of metabolic rate), to identify the metabolites, and to detect which enzymes are responsible for the metabolism of the drug. Compounds that are excreted out of the body at high rates will result in a drug with short duration and requiring multiple daily dosing. On the other hand, compounds that have very slow metabolic rates lead to high levels of the drug in the body for extensive period. Since the compound is being chemically modified in the metabolic process, it is important to identify the metabolites and, in some cases, test the biological activity and toxicity of these metabolites. Human beings are constantly consuming different kinds of chemical substances and the majority of them are taken directly to the liver to be metabolized. If more than one compound competes for the same metabolic enzymes, the rate of metabolism of these compounds could be affected.

This phenomenon is called drug-drug interaction, and must be understood when dosing a patient with multiple drugs (Di, 2011).

Human Liver Metabolism: Cytochrome P450

The majority of drugs that are currently in the market are cleared by metabolism in the liver. Orally administered drugs are transported through the portal vein to the liver, which is why the liver is called the primary site of metabolism. When compounds enter the liver to be metabolized, the chemical process that they undergo is divided in two phases: Phase I metabolism and phase II metabolism (Di, 2011). In phase I metabolism, the compound undergoes predominantly a free-radical hydroxylation reaction. This chemical process is catalyzed by enzymes called cytochrome P450 (CYP) and uses NADPH as a cofactor (Danielson, 2002). The purpose of the phase I metabolism is to hydroxylate the substrate to increase the polarity of the compound, making it more water soluble, hence facilitating the excretion of the drug by the kidney. Once phase I of the metabolism is completed, the product obtained is called a metabolite and it can undergo a second chemical reaction that has as a goal to further functionalize the added hydroxyl group to enhance polarity and excretion (Di, 2011). This is called phase II metabolism, and involves adding sulfates, glucuroidates, etc. to the hydroxyl to further increase water solubility. Phase I metabolism is the rate limiting step (Di, 2011). **Figure 6** shows the schematic diagram of drug metabolism in the liver, including phase I and phase II.

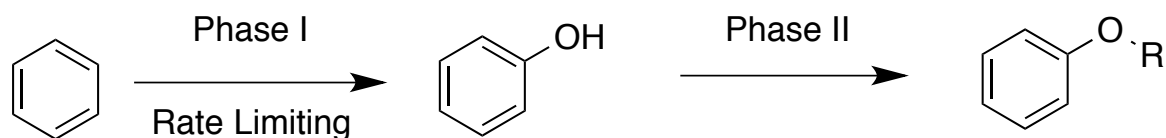


Figure 6. Liver metabolism of drugs. Benzene works as an example of a drug that through phase I gets hydroxylated by cytochrome p450 enzymes. Through phase II, the hydroxyl group gets further functionalized. The R group represents sulfates, glucuroides, amongst other.

It has been found that 75% of marketed drugs are metabolized in the liver by cytochrome P450 (Turpeinen, 2005). This family of enzymes is the terminal oxidase enzymes in electron-transfer chains (Danielson, 2002). Cytochrome p450 enzymes are present in the liver and act as the catalysts for the phase I metabolism by binding to the substrate and NADPH as cofactor (Danielson, 2002). **Figure 7** shows the condensed catalytic cycle by CYP – which corresponds to phase I metabolism of drugs in the liver. In this catalytic cycle, the purpose is to hydroxylate the compound to increase polarity and enhance renal excretion, and it requires two electrons coming NADPH (electron transfer chain).

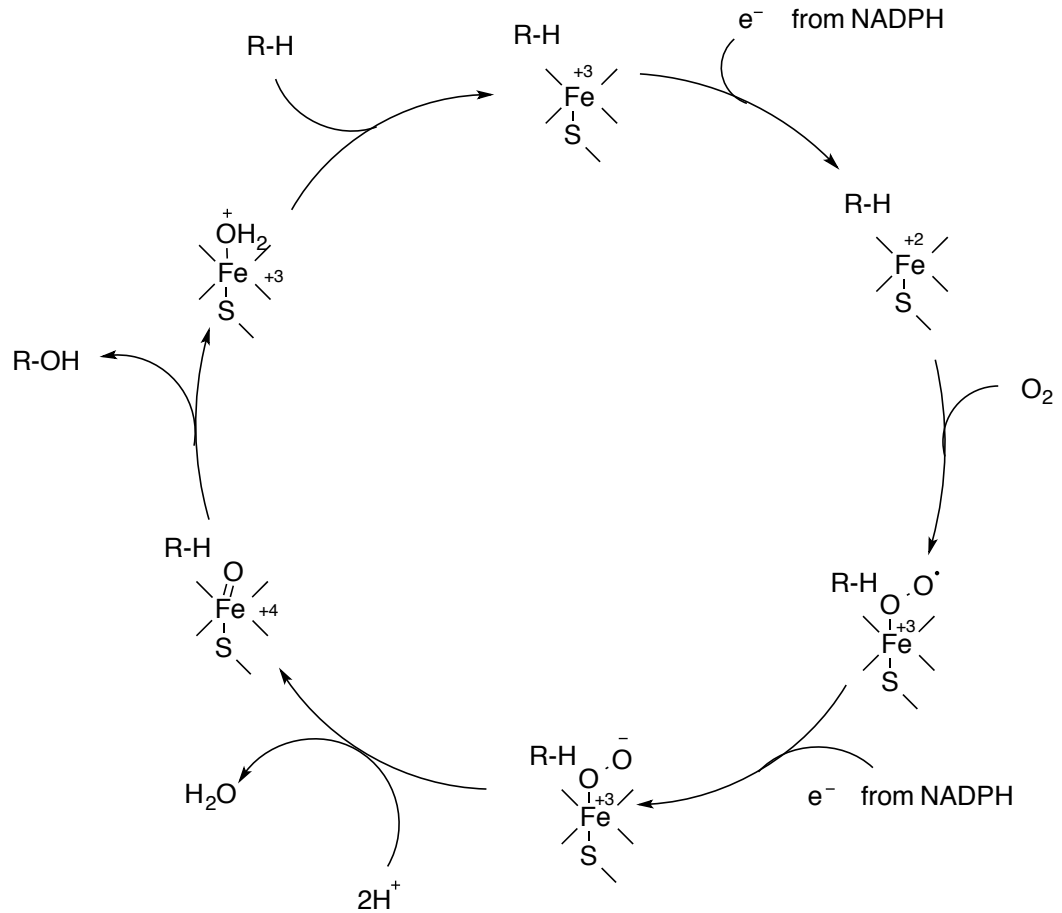
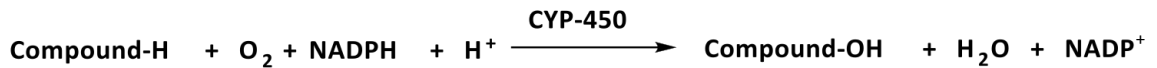


Figure 7. Condensed catalytic cycle by CYP family in the liver. R-H represents the drug entering the catalytic cycle. This cycle is the responsible for the phase I metabolism in the liver. The substrates enters the cycle and the product is a hydroxylated compound.

The hydroxylation reaction of phase I metabolism is represented by the following equation:



As stated before, cytochrome p450 is a family of oxidase enzymes – thus, there are different isozymes amongst CYP. Isozymes are enzymes that catalyze the same reaction but differ in their amino acid sequence, which suggests that, each one of them could show different specificity and affinity toward various substrates (Weiss, 1977).

Since the polypeptide chain is different for each isozyme, a drug can bind to a specific isozyme in the liver to be metabolized. However, more than one drug can show specificity toward the same isozyme (CDER, 1997), which could result in drug-drug interactions. Thus, in drug discovery, it is important to determine which isozyme is responsible for the phase I metabolism in order to predict if drug-drug interactions will arise. Identification of the isozyme that metabolizes a drug can be done with the use of the isozyme's inhibitor, following the metabolism of the compound of interest in presence of the inhibitor. **Table 3** presents the inhibitors for some of the different cytochrome p450 isozymes.

Isozyme	Inhibitor
CYP 1A2	Cimetidine, Amiodarone, Ticlopidine
CYP 2C19	Cimetidine, Ketoconazole, Omeprazole
CYP2C9	Fluvastatin, Lovastatin, Isoniazid
CYP 2D6	Cimetidine, Fluoxetine, Methadone
CUP 2E1	Disulfiram, Water Cress
CYP 3A4,5,7	Cimetidine, Iarithromycin, Ketoc nazole

Table 3. Cytochrome p450 isozymes and their corresponding inhibitors.

In vitro human metabolism: Microsomes

Phase I metabolism can be followed *in vitro* using human liver microsomes. These microsomes mimic small structures within the cell, contain CYP enzymes, and are made from pieces of endoplasmic reticulum (CDER, 1997). Microsomes are not found in living

organisms, but are formed when the CYP enzymes are isolated from liver cells. Liver microsomes are used in the pharmaceutical industry to study the phase I metabolism of compounds (Voet, 2004). Human liver microsomes contain cytochrome p450, thus they allow the study of *in vitro* metabolic rates, identification of metabolites and detection of the CYP isozyme responsible for the phase I metabolism. When performing *in vitro* studies, intrinsic clearance is calculated which represents the metabolic rate. Intrinsic clearance is the intrinsic capacity of the microsomes to metabolize a drug by phase I metabolism (Woosley, 1984). Lower intrinsic clearance implies that the liver has less ability to metabolize the drug; hence it suggests slower metabolic rates. The goal is for our compounds to have *in vitro* intrinsic clearance similar to those of the marketed drugs. **Table 4** presents *in vitro* intrinsic clearance range used to rank compounds from low clearance to high (Barter, 2007).

Clearance Category	Intrinsic Clearance ($\mu\text{L}/\text{min}/\text{mg}$ protein)				
	Human	Monkey	Dog	Rat	Mouse
Low	< 8.6	< 12.5	< 5.3	< 13.2	< 8.8
High	> 47.0	> 67.8	> 28.9	> 71.9	> 48.0

Table 4. Classification of compounds into low or high intrinsic clearance depending on the species. The difference in ranges is due to the fact that there exist an inherent difference in CYP40s and circulatory systems rates among species.

Modification of Metabolic Rates

Metabolic stability is essential for a drug to have an acceptable pharmacokinetic profile. Metabolic stability has an inverse relation to the intrinsic clearance of the drug; as the metabolic stability decreases, the intrinsic clearance increases. Thus, the pharmacokinetics of a drug determines the frequency of dosing (Di, 2011). Through the years, medicinal chemists have developed a series of strategies to improve metabolic stability using structural modifications to inhibit phase I metabolism in the liver. Strategies such as blocking metabolic sites, changes in ring substituents, chirality, and functional groups have been used in the industry for the past few decades. One of the most frequently used strategies to improve metabolic profiles is to reduce the rate of hydroxylation by addition of a fluorine atom. Fluorine is less reactive than the hydrogen that was in the metabolite site of the lead structure (Di, 2011). As an electron-withdrawing group (i.e. a strong C-F bond), fluorine slows the free radical hydroxylation by CYP. F is small and has little effect on the size of the molecule.

The rate of free-radical hydroxylation by cytochrome p450 has been correlated with electron density in the molecular portion being metabolized (Galetin, 2006). Moieties containing electron-withdrawing groups usually have slower rates of metabolism. Thus, improved metabolic profiles can be achieved by adding fluorine to lead structures. In 2004, Nassar et al. modified a series of compounds and evaluated the effects on metabolic rates. An orally administered antiviral agent (**Figure 8**) was modified by reducing the rate of hydroxylation at the vulnerable site of metabolism by

adding a fluorine substituent. The new compound was tested *in vivo* and the authors then observed an increase in the percent bioavailability, which is inversely related to metabolic rate. The fluorine substituent did not affect the biological potency, IC_{50} , but reduced the metabolic rate (clearance) as measured by percent bioavailability, %F. The increase in percent bioavailability – measured *in vivo* – suggests that the structural modification of adding the fluorine increased the half-life of the compound and decreased its intrinsic clearance.



Figure 8. Modification of metabolically labile group by substitution with fluorine in an orally administrated vinylacetylene antiviral. %F is a measure of the *in vivo* bioavailability. IC_{50} is a measure of the antiviral potency.

The effect of structural changes on *in vitro* metabolic stability using human liver microsomes is routinely performed in the pharmaceutical industry to initially evaluate human metabolism.

The Doll lab has identified two structural classes that reactivate mutant p53 in human cancer cells and are shown in **Figure 9**. The benzimidazole compound (A) was disclosed in a 2010 patent as a compound that bound to wild type p53 (Dasmahapatra, 2010). However, nothing was said about reactivating mutant p53. The quinoline

compound (B) was disclosed in a 2010 patent that claimed the inhibition of angiogenesis (growth of blood vessels) by blocking the protease MetAP2 (Liu, 2009). Since p53 will inhibit angiogenesis as well, it was conceivable that compound (B) might also be acting through a p53 reactivation mechanism. Doll's lab has shown that both of these compounds (A and B) do indeed reactivate mutant p53 in human tumor cells.

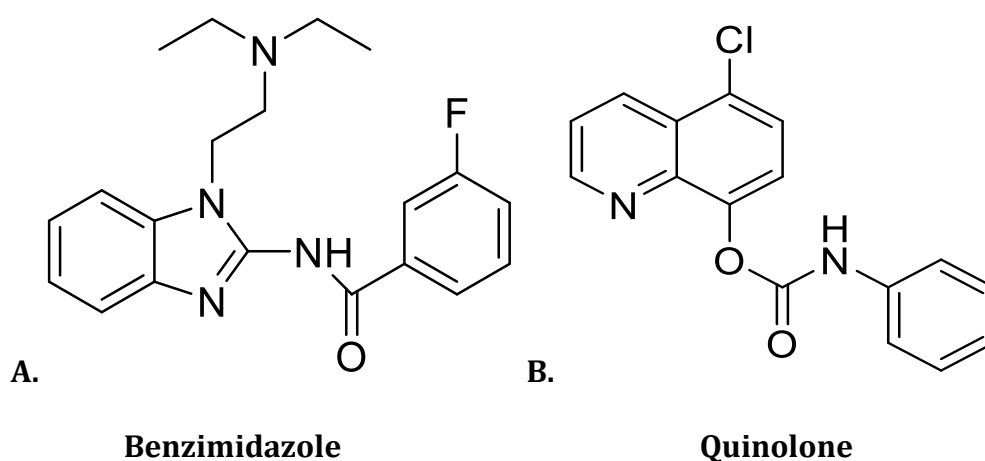


Figure 9. Examples of benzimidazole (A) and quinolones (B) class of compounds, respectively that reactivate mutant p53 in human tumor cells. Compounds of type A were shown to bind to wild type p53 (US patent 7,790,474 (2010)). Compounds of type B were shown to inhibit angiogenesis by inhibiting the protease MetAP2. (WO 2010/042163 A2)

First, benzimidazoles are heterocyclic aromatic organic compounds that result from the joining of benzene and imidazole rings. Many marketed drugs (e.g., Albenza and Egaten, which are in the group of orally administrated anthelmintic drugs; Mebendazole, which is a drug used to treat a number of parasitic worm infestations;) are in the benzimidazole class of compounds (Barker, 1960).

The second class of compounds, quinolines, consists of synthetic compounds that were originally found to act as antibacterial drugs and are composed by two heterocyclic aromatic systems (Andriole, 1989).

This study describes efforts to develop a compound in the benzimidazole class that not only binds to and reactivates mutant p53 in human cancer cells, but also that exhibits drug-like properties such as membrane permeability, low toxicity, high bioavailability, and metabolic stability, among others.

RESEARCH OBJECTIVES

In the drug discovery context, our overall goal is to design and optimize compounds that bind to and reactivate mutant p53 in human cancer cells. As a step towards the goal in the drug discovery framework, we are exploring the two main drug-like properties of our compounds, which are human metabolic stability and membrane permeability (Walker, 2006). Specifically, my research is concentrated on the *in vitro* human metabolic profile of compounds that have been shown by our group to reactivate the mutant protein, p53. This includes determining the *in vitro* intrinsic human clearance (metabolic rate) of our compounds, comparing it to those of marketed drugs, and determining the human metabolites. Understanding the human metabolites allows us to make structural changes in our compounds to adjust the *in vitro* intrinsic human clearance to better match those of marketed drugs.

Using our lead structures identified to have biological activity towards reactivation of mutant p53 in human cancer cells, the goal is to design and synthesize structurally modified compounds to improve metabolic stability while maintaining the desired biological activity. The experimental process is to incubate the lead compounds with human liver microsomes and NADPH, then calculate *in vitro* human intrinsic clearance and identify metabolites of phase I metabolism. Using *in vitro* metabolic data from the lead structures, we can then design analogs with structural changes that would allow for a slower metabolic rate and more metabolically stable compounds

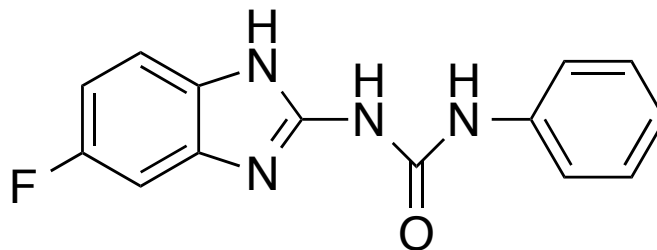


Figure 10. 1-(5-fluorine-1H-benzo[d]imidazole-2-yl)-3-phenylurea. Example of the benzimidazole class of compounds with an added fluorine moiety. This examples illustrates a structural change made to a lead structure found to reactivate mutant p53 in human cancer cells in Doll's Lab.

The benzimidazole class of our mutant p53 reactivator compounds is the focus of this work (**Figure 10**). By adding an electron-withdrawing group to the benzimidazole portion of the structure, we believe that the catalytic reaction by CYP will be slowed. It is known that CYP enzymes show high affinity for electron-rich systems (Galetin, 2006); hence, fluorine as an electron-withdrawing group should increase the metabolic stability of the compound. To further demonstrate this hypothesis, compounds containing electron-donating group – such as methyl, will be synthesized. These compounds should decrease the metabolic stability by increasing affinity of CYP for the substrate.

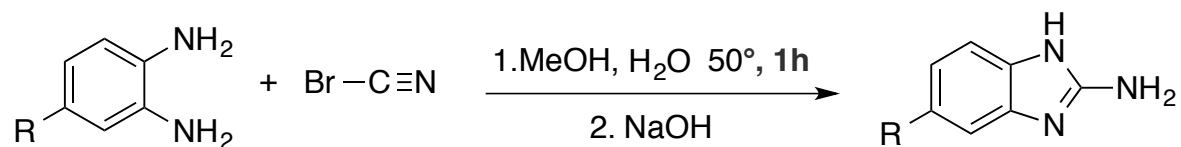
In summary, the goal is to determine the *in vitro* human intrinsic clearance of our compounds and identify the metabolites. If the clearance rate is low or lower than marketed drugs, we plan to introduce structural changes to the compound so as to decrease the *in vitro* intrinsic clearance. To demonstrate our hypothesis, we also plan to introduce structural changes that should increase the *in vitro* intrinsic clearance. The metabolic stability data collected will be analyzed to identify the category of the clearance according to the ranges described in **Table 4** for humans – each compound will

be characterized as low, medium, or high *in vitro* intrinsic clearance. Structural changes will be evaluated to establish a Structural Activity Relationship (SAR), taking into consideration possible implications of structural changes in other drug-like properties, such as membrane transport rate.

EXPERIMENTAL SECTION

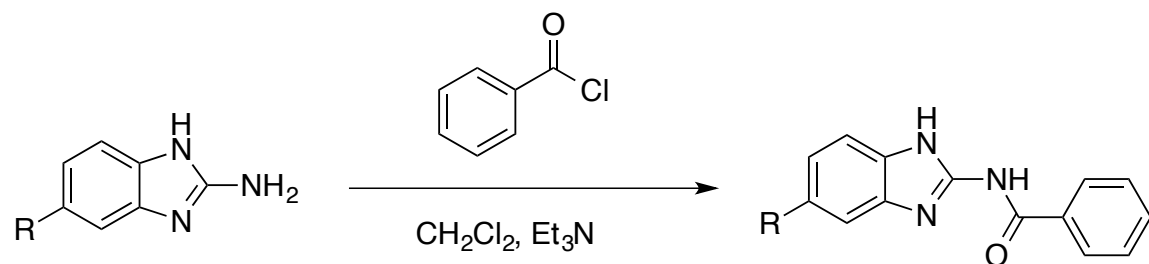
Synthetic Strategies

Synthesis of Intermediates



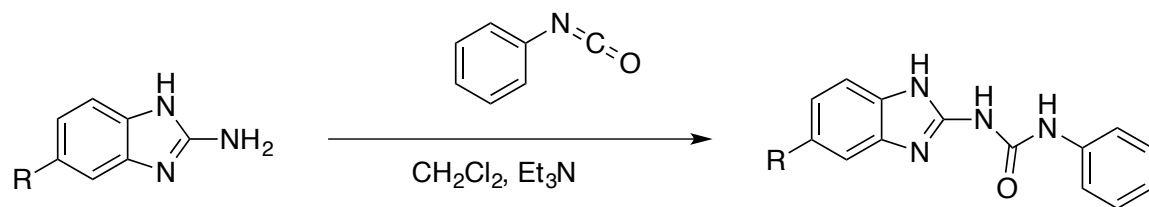
Scheme 2. Synthesis of intermediates, where R represents fluorine or a methyl, depending on the desired product. Procedure taken from H. Blackwell, *et al.* US Pat Ap 20130136782 (2013).

Synthesis of Amides



Scheme 3. Synthesis of amide benzimidazoles, where R represents fluorine or methyl to yield the desired product.

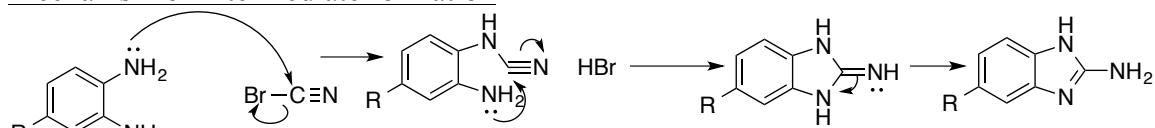
Synthesis of Ureas



Scheme 4. Synthesis of urea benzimidazoles, in which R represents fluorine or methyl, depending on the desired product.

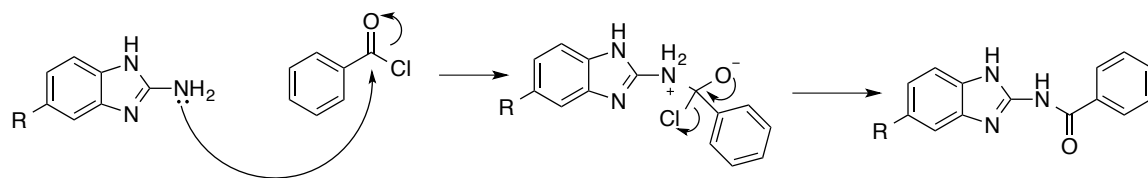
Mechanisms of Above Reactions

Mechanism of Intermediate formation



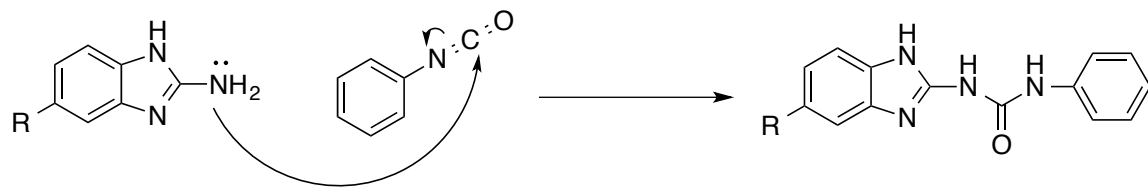
Scheme 5. Mechanism for the synthesis of intermediates, where R represents fluorine or a methyl, depending on the desired product.

Mechanism of Amide formation



Scheme 5. Mechanism for the synthesis of amides, where R represents fluorine or a methyl, depending on the desired product.

Mechanism of Urea formation



Scheme 7. Mechanism for the synthesis of ureas, where R represents fluorine or a methyl, depending on the desired product. The proton in the $-NH_2$ migrates to the N position in the isocyanate group.

Reagents

Benzimidazole compounds, three analogs, were synthesized in the laboratory, supplied with reagents purchased from Sigma-Aldrich and Acros. Human liver microsomes (pooled male, 10mg/\$190 used as is from BioreclamationIVT, 410-455-1242). and NADPH were purchased from Sigma-Aldrich as well.

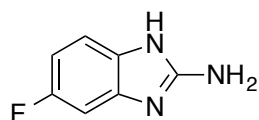
Characterization

All synthesized compounds were characterized by nuclear magnetic resonance (NMR) and liquid chromatography coupled with mass spectroscopy (LC/MS) for purity and structure verification.

NMR spectra were recorded on a 400 MHz, Bruker instrument, TopSpin 2.1.6 Software, ICON-NMR 2.0 Automation Software with autosampler. Dimethyl sulfoxide (DMSO) was used as a solvent for all NMR spectra. Chemical shifts were expressed in ppm (δ) relative to Tetramethylsilane (TMS), the accepted standard for calibrating chemical shift in NMR spectra. LC/MS were recorded on a Waters Time of Flight, Micromass LCT mass spectrometer coupled to an Agilent 1100 HPLC, with a syringe pump, API Probe and datastation MassLynx. The HPLC column was an Analytical, Echelon 100 x 4.6 mm C18 column with an acetonitrile (ACN)-water mobile phase flow rate of 1.5 mL/min and the following gradient: 0 min 30% ACN, 8 min 70% ACN, 9 min 70% ACN, 11 min 80% ACN, 12 min 85% ACN, 13 min 30% ACN, 15 min 30% ACN. Purified and characterized compounds were designated with "RD numbers", sequential numbers given to compounds from Ronald Doll's laboratory, and stored in glass containers at room temperature.

Synthetic Pathways

Synthesis of Intermediates



5-fluoro-2-aminobenzimidazole. This intermediate was synthesized according to the US Patent Application #20130136782. 4-fluoro-1,2-diaminobenzene (1.0 g, 5.35 mmol, 1.0 eq.) was dissolved in a 1:1 mixture of MeOH (40 mL) and water (40 mL) in a 250mL round bottom flask. The reaction mixture was treated with cyanogen bromide (ACROS, 1.7 g, 16.04 mmol, 3 eq.) and heated at 50°C for one hour and 45 minutes. After cooling to room temperature, the reaction mixture was concentrated by removing MeOH in vacuum. The remaining mixture was basified with 1.0 M aq. NaOH until pH>8.0, and extracted with EtOAc (3x30 mL). The remaining organic mixture was washed with water (2x50 mL), brine (50 mL), dried over MgSO₄ and concentrated in vacuum to yield 5-fluoro-2-aminobenzimidazole. The product was then triturated with three portions of hexanes (3x10 mL) to yield (0.89±0.01) g (5.88 mmoles) of a brown solid that was used without further purification.

Percent yield: > 100% (product is not purified).

m/z: . 151.05 (95.0%), 152.06 (7.6%)

Percent purity by HPLC: 91%

NMR 400 MHz, ¹H NMR, DMSO: 10.75 ppm (1 H, s, a); 6.99 ppm (1 H, d, 1); 6.89 ppm (1 H, d, 3); 6.65 ppm (1 H, t, 2); 6.25 ppm (2 Hs, s, b).

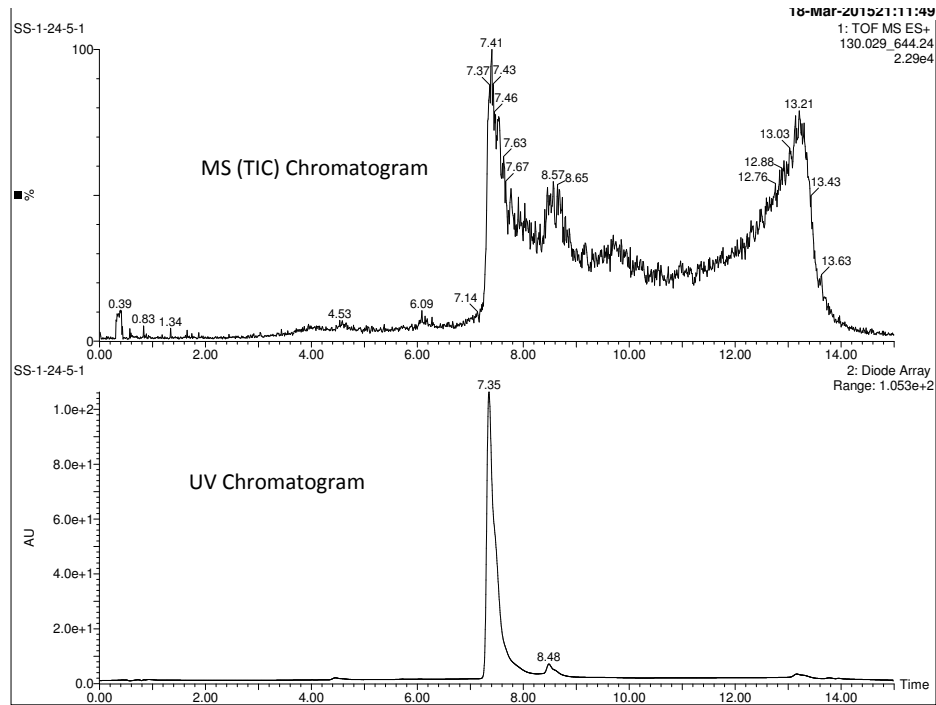


Figure 11. Liquid chromatogram for **5-fluoro-2-aminobenzimidazole**

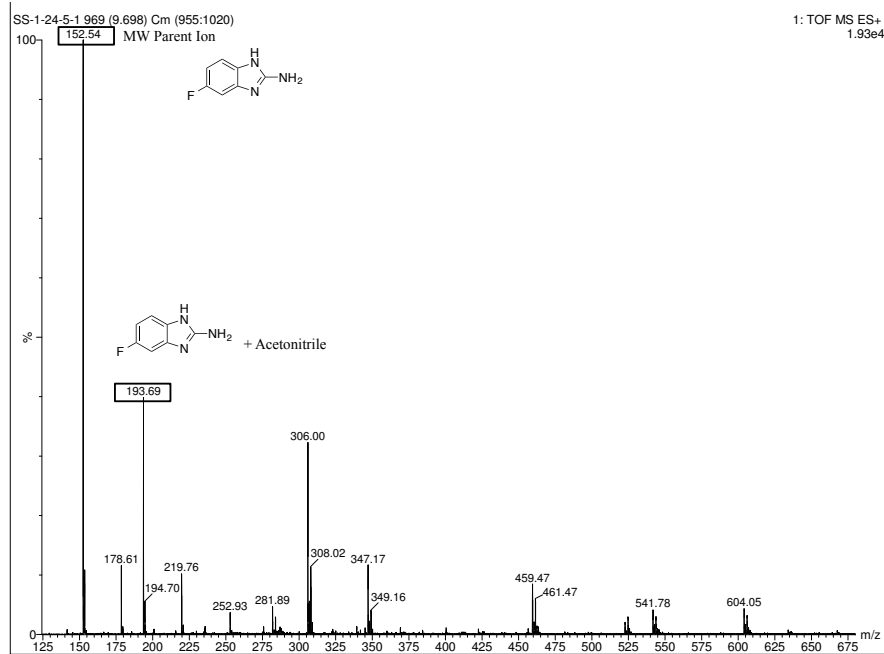


Figure 12. Mass spectrum for **5-fluoro-2-aminobenzimidazole** from peak at 7.41 minutes in TIC chromatogram on **Figure 11**.

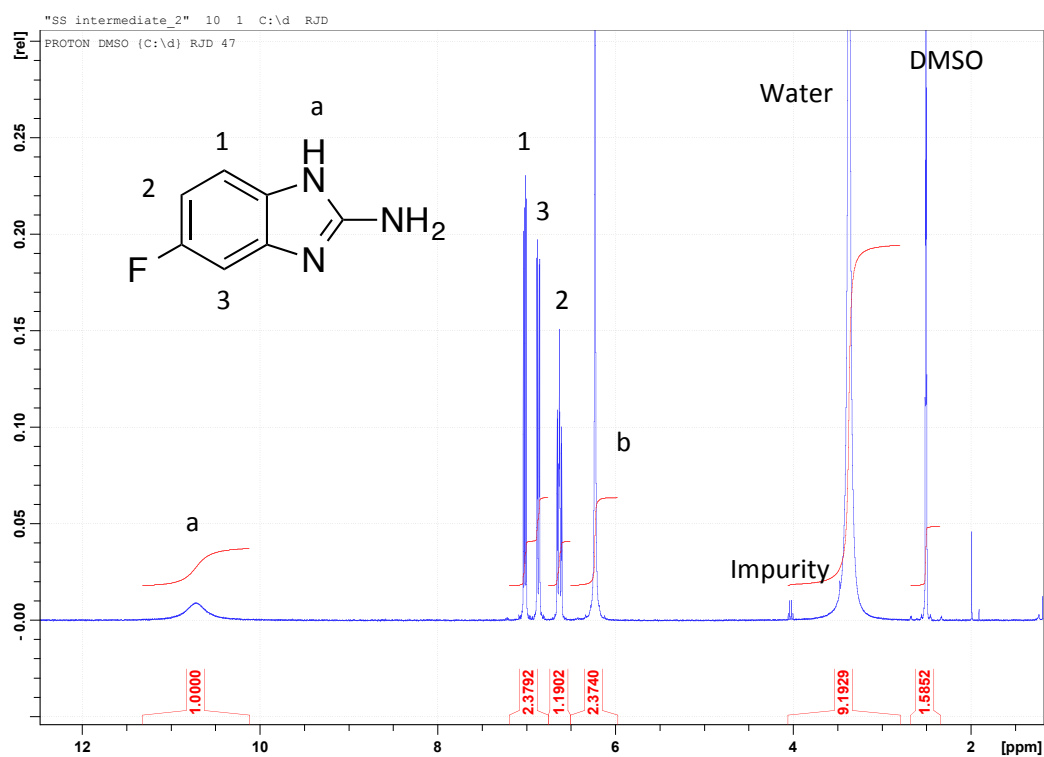
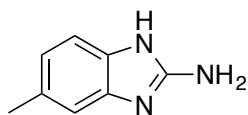


Figure 13. NMR spectrum of **5-fluoro-2-aminobenzimidazole**. Proton **a** is in a more aromatic magnetic environment, thus it is more deshielded. Furthermore, the effect of fluorine as an electron-withdrawing group further deshields proton **a**. On the other hand, proton **b** is more shielded and it is a single that integrates to 2. In the literature, it has been observed that -NH_2 in benzimidazoles show around 6 ppm.



5-methyl-2-aminobenzimidazole was synthesized following the same procedure but using 4-methyl-1,2-diaminobenzene (1.0 g, 8.19 mmol, 1.0 eq.) as the reagent instead of 4-fluoro-1,2-diaminobenzene, with molar ratios as described for the synthesis of 5-fluoro-2-aminobenzimidazole. The product was then triturated with three portions of hexanes

(3x10 mL) to yield (0.97±0.01) g (6.59 mmoles) of a brown solid that was used without further purification.

Percent yield: 81 %

m/z: 147.08 (100.0%), 148.08 (8.7%)

NMR 400 MHz, ¹H NMR, DMSO: 8.65 ppm (1 H, s, a); 7.45 ppm (2 Hs, d, b); 7.25 ppm (2 Hs, t, 1,3); 6.95 ppm (1 H, t, 2); 2.5 ppm (3 Hs, s, 4). Proton b on **Figure 17** appears to show splitting; however, this is not splitting due to coupling. The behavior for the peak of proton b is due to the fact that more tautomers (**Figure 15**) are stable due to the donation of electron density from the methyl substituent.

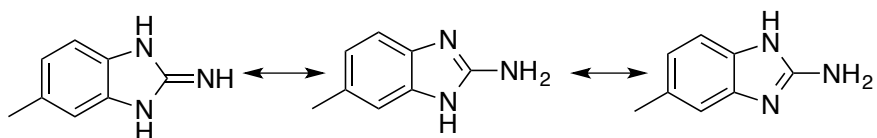


Figure 14. Possible tautomers for **5-methyl-2-aminobenzimidazole** that experience enough stabilization due to donation from the methyl that multiple peaks in the NMR life-time are observed for the -NH₂ protons.

Percent purity by HPLC: 91%

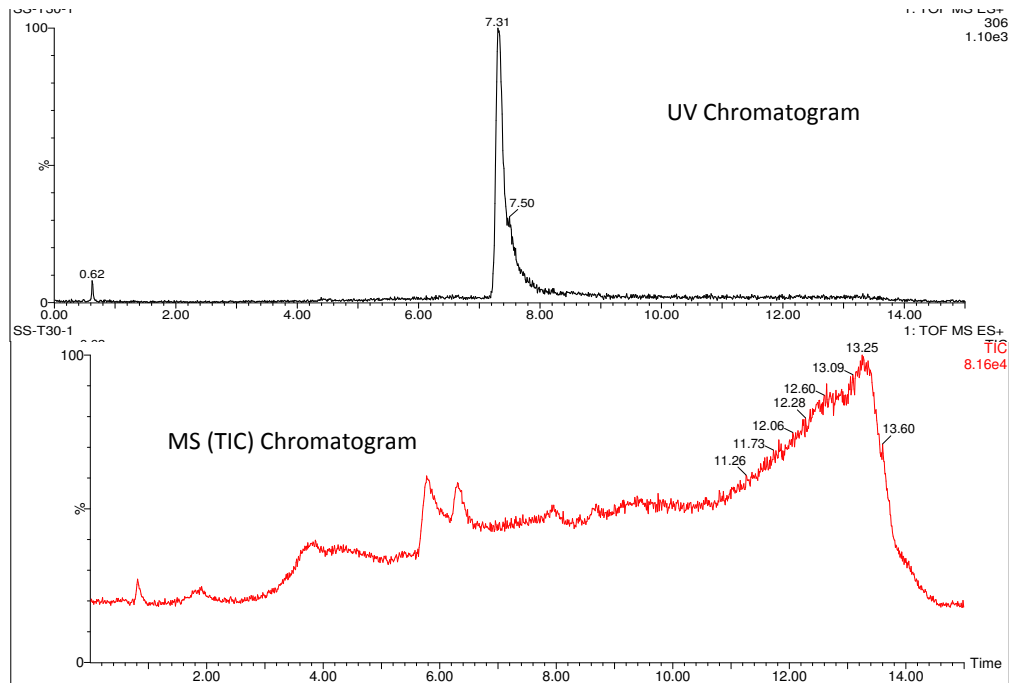


Figure 15. Liquid chromatogram for **5-methyl-2-aminobenzimidazole**. The ionization efficiency by MS is low for this compound.

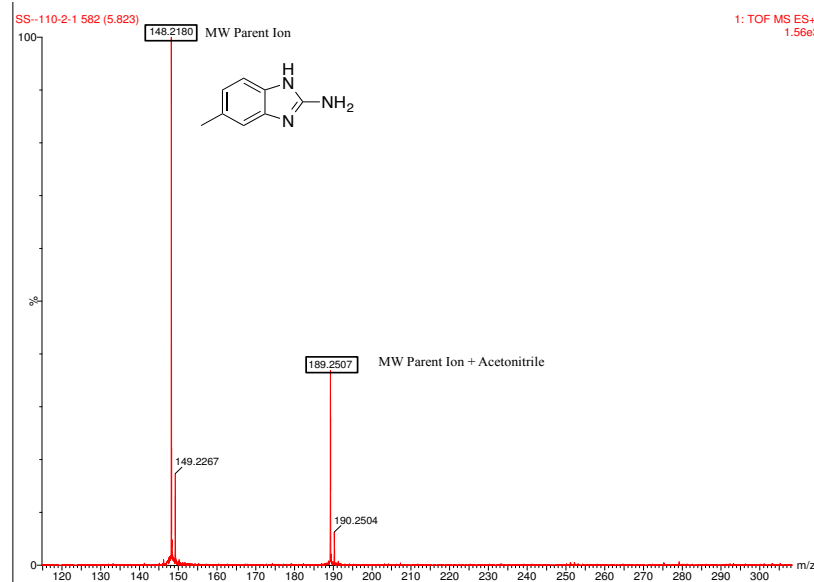


Figure 16. Mass spectrum for **5-methyl-2-aminobenzimidazole** from peak 7.31 minutes in TIC chromatogram in **Figure 15**.

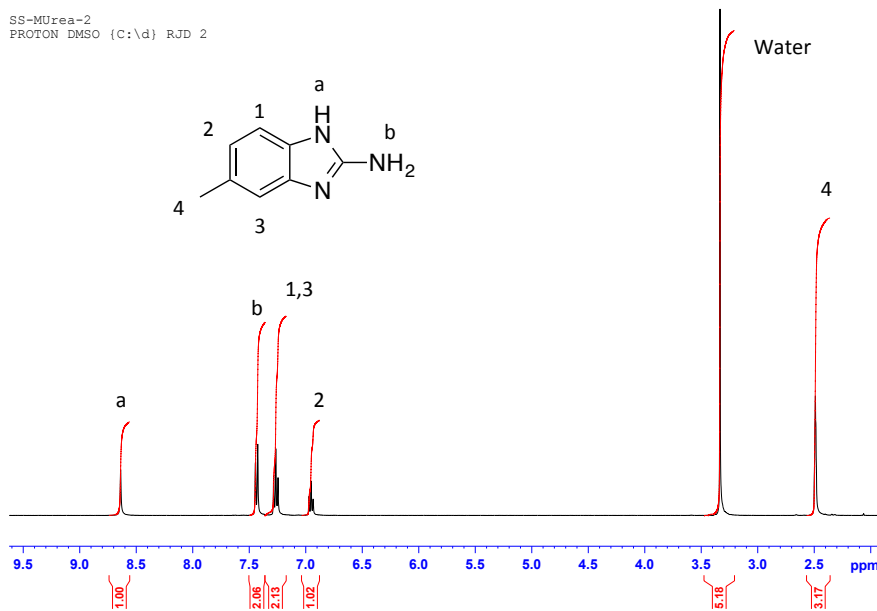
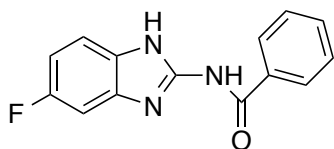


Figure 17. NMR spectrum of **5-methyl-2-aminobenzimidazole**. The effect of methyl as an electron-donating group causes proton a to be more shielded compared to the fluorinated benzimidazole. Proton b shows evidence of tautomers.

Synthesis of Amides



***N*-(5-fluoro-1*H*-benzo[d]imidazole-2-yl)benzamide: RD 78.** A 100ml RB flask was charged with 5-fluoro-2-aminobenzimidazole (0.1 g, 0.66 mmole) and dissolved in 12 mL dichloromethane (CH_2Cl_2). To the resultant mixture, triethylamine (Et_3N) (0.1 mL, 0.72 mmole) was added along with benzoyl chloride (0.1 mL, 0.86 mmole), both in excess. The reaction was stirred overnight. The solution was transferred into a separatory funnel and the flask was washed with methylene chloride. Aqueous sodium bicarbonate

was added and the organic layer was then separated. The remaining organic solution was washed with brine and water. The solution was concentrated under vacuum. Recrystallization was performed using 50:50 ethyl acetate and hexanes solvents to yield (0.34±0.01) g (1.33 mmoles) of a white solid.

Percent yield: 97 %

m/z: 255.08 (100.0%), 256.08 (15.1%), 256.08 (1.1%), 257.09 (1.1%)

NMR 400 MHz, ¹H NMR, DMSO: 12.5 ppm (2 Hs, s, a,b); 8.15 ppm (2 Hs, d, o); 8.00 ppm (1 H, d-d, m); 7.5 ppm (3 Hs, m, 1,2,3); 7.00 ppm (1H, d-d, p). The presence of fluorine as an electron-withdrawing group in the benzimidazole portion of the compound favors and stabilizes the “enol” conformation around the C-N single bond in the structure. Thus, the two rotamers are observed in the NMR life-time.

Percent purity by HPLC: 97%

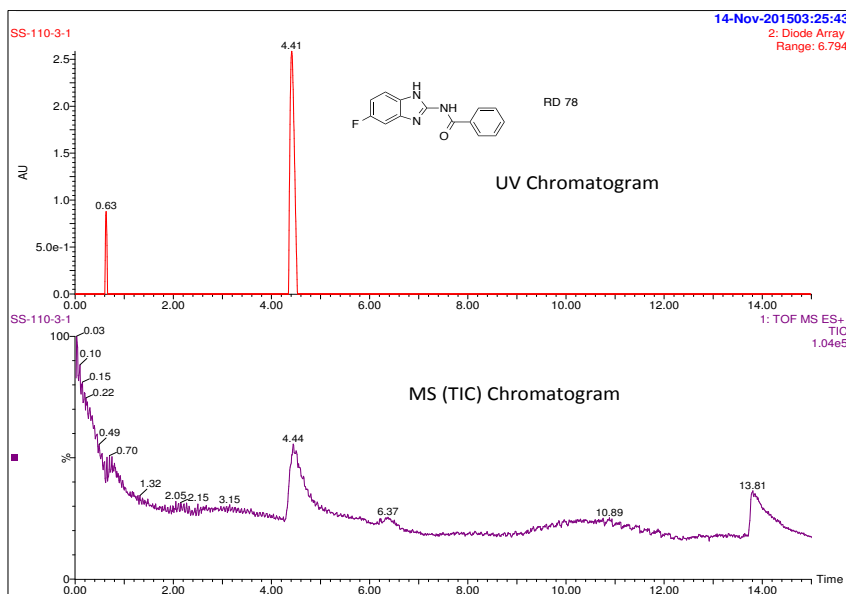


Figure 18. Liquid chromatogram for *N*-(5-fluoro-1*H*-benzo[d]imidazole-2-yl)benzamide

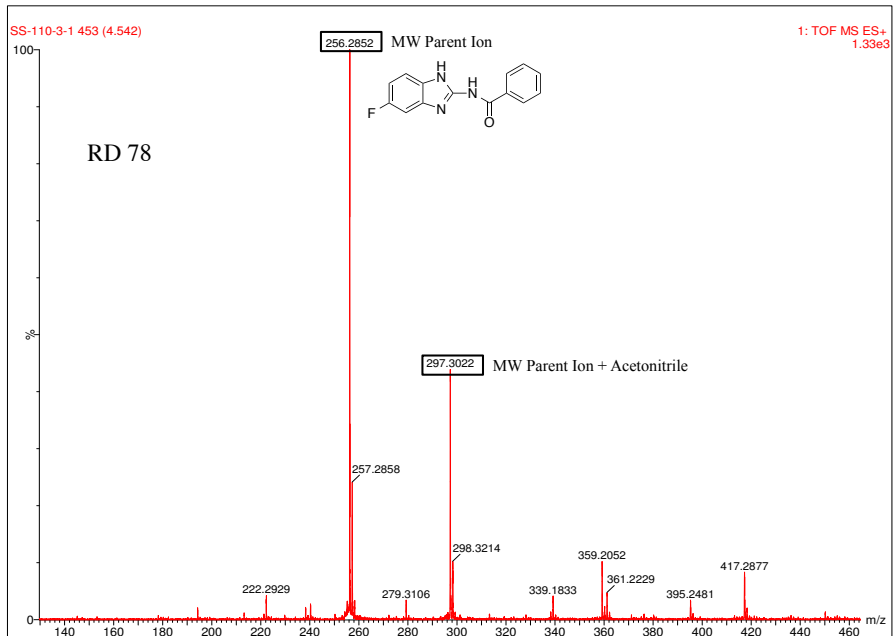


Figure 19. Mass spectrum for *N*-(5-fluoro-1*H*-benzo[d]imidazole-2-yl)benzamide for peak at 4.41 minutes on TIC chromatogram on **Figure 18**.

RD 78

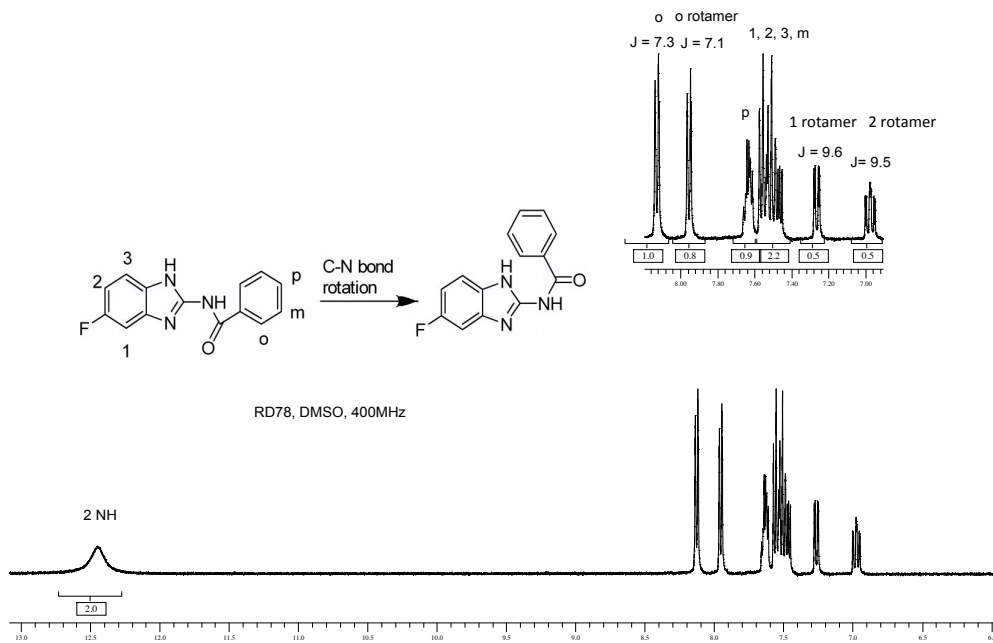
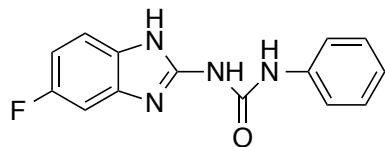


Figure 20. NMR spectrum of *N*-(5-fluoro-1*H*-benzo[d]imidazole-2-yl)benzamide.

Synthesis of Ureas

1-(5-fluoro-1H-benzimidazole-2-yl)-3-phenylurea: RD 86. The procedure for the synthesis of the ureas was analogous to that of the amides; instead of adding benzoyl chloride to the reaction mixture, phenyl isocyanate (1.00 g, 7.14 mmol) was used as the reagent in the same molar ratios as in the amides' procedures. Recrystallization was performed using acetonitrile to yield (0.87±0.01) g (3.22 mmol) of a white solid.

Percent yield: 97%

m/z: 270.09 (100.0%), 271.10 (15.1%), 271.09 (1.5%), 272.10 (1.1%)

NMR 400 MHz, ¹H NMR, DMSO: 12.5 ppm (2 Hs, s, b, c); 8.1 ppm (2Hs, d, o); 7.9 ppm (2Hs, d-d, m); 7.5 ppm (3 Hs, m, 1,2,p); 7.3 ppm (1 H, s, a); 7.0 ppm (1H, s, 3).

Analogous to the amide compound, the hindered rotation is observed around the C-N bond, showing two rotamers for this compound. The two hydrogens missing for the NH groups can be explained due to the rapid exchange between these protons and water with DMSO as a solvent. As a result, the large difference in chemical shifts causes the -NH peaks to be so broad that they are indistinguishable from the baseline.

Percent purity by HPLC: 100%

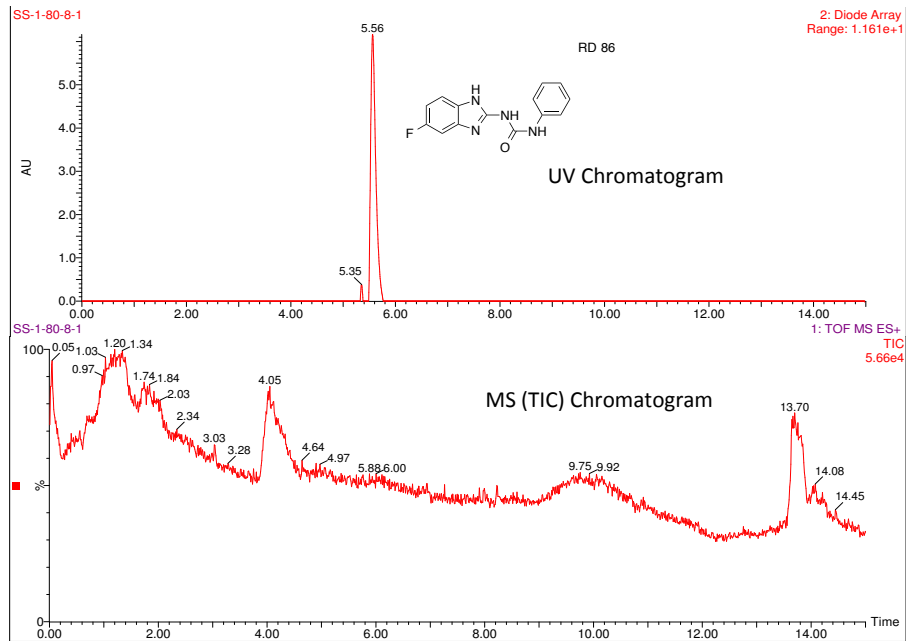


Figure 21. Liquid chromatogram for 1-(5-fluoro-1H-benzo[d]imidazole-2-yl)-3-phenylurea. The ionization efficiency by MS is low for this compound.

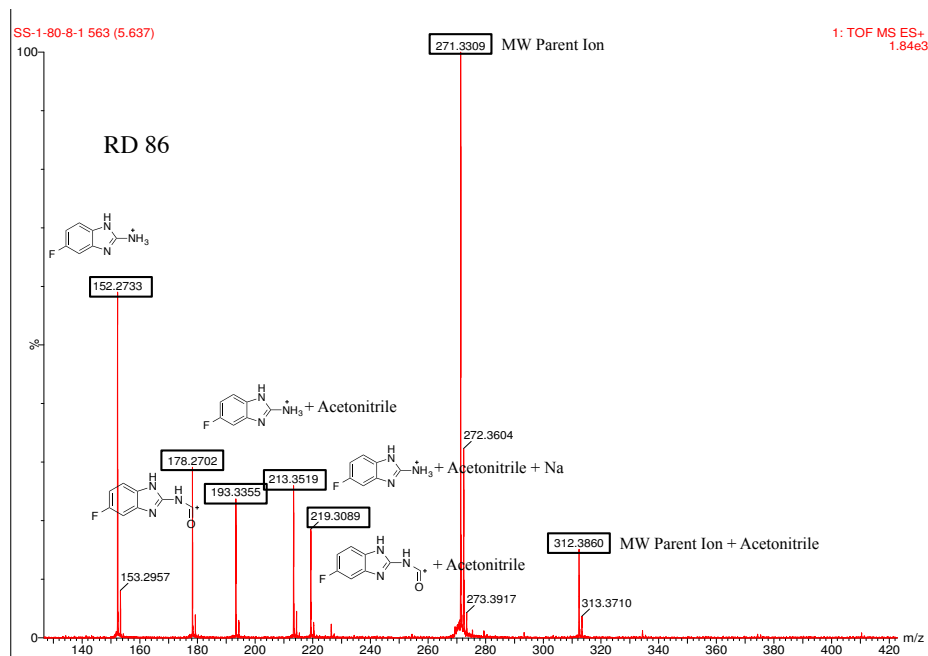


Figure 22. Mass spectrum for 1-(5-fluoro-1H-benzo[d]imidazole-2-yl)-3-phenylurea from peak 5.56 minutes of TIC chromatogram on Figure 18.

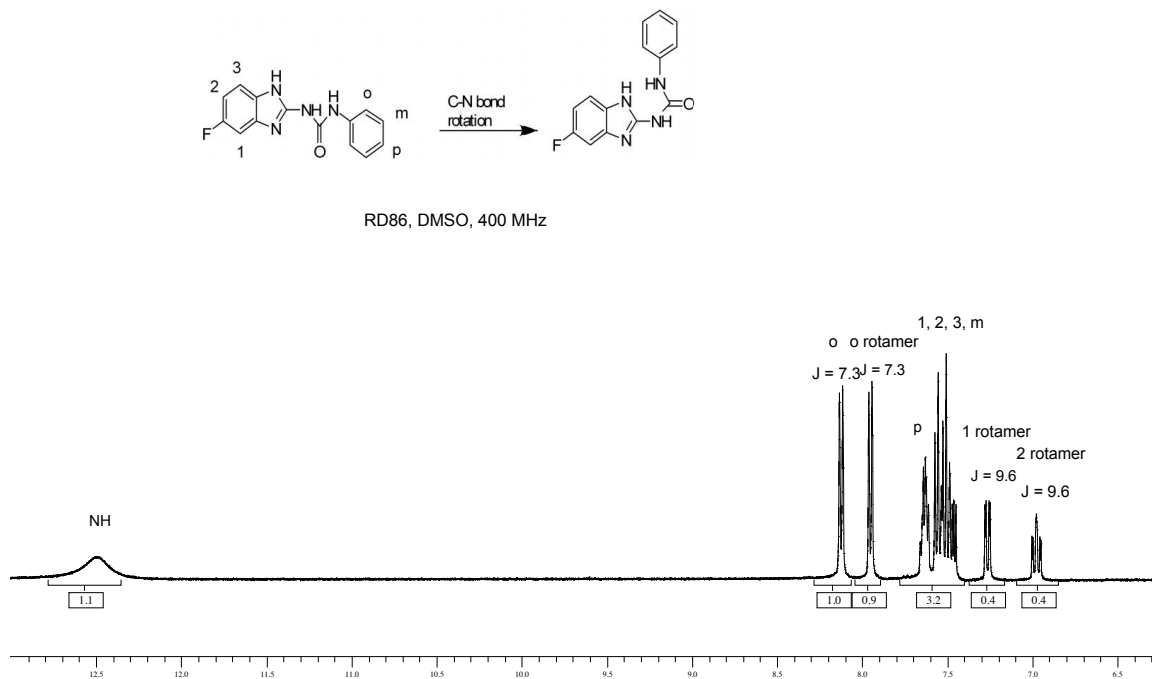
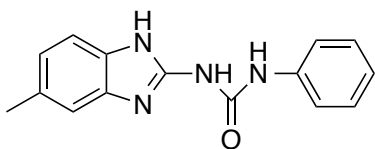


Figure 23. NMR spectrum for **1-(5-fluoro-1H-benzo[d]imidazole-2-yl)-3-phenylurea**



1-(5-methyl-1H-benzo[d]imidazole-2-yl)-3-phenylurea: RD 89. The procedure for the synthesis of the ureas was analogous to that of the amides; instead of adding benzoyl chloride to the reaction mixture, isocyanatobenzene was used as the reagent, in the same molar ratios as in the amides' procedure. Recrystallization was performed using acetonitrile to yield (0.74±0.01) g of a white solid.

Percent yield methyl: 81%

m/z: 266.12 (100.0%), 267.12 (16.2%), 267.11 (1.5%), 268.12 (1.2%)

NMR 400 MHz, ^1H NMR, DMSO: 11.9 ppm (1H, s, a); 10.1 ppm (1H, s, b); 10.75 ppm (1H, s, c); 8.35 ppm (2 Hs, d-d, m); 7.50 ppm (2Hs, m, o,p); 6.99 ppm (2 Hs, m, 1,3); 6.5 ppm (1H, m, 2); 5.00 ppm (3 Hs, s, 4). No hindered rotation was observed for this compound; a possible explanation lies in the fact that the presence of methyl as a substituent does not stabilize the “enol” conformation enough for the NMR to distinguish the two conformations around the C-N single bond.

Percent purity by HPLC: 95%

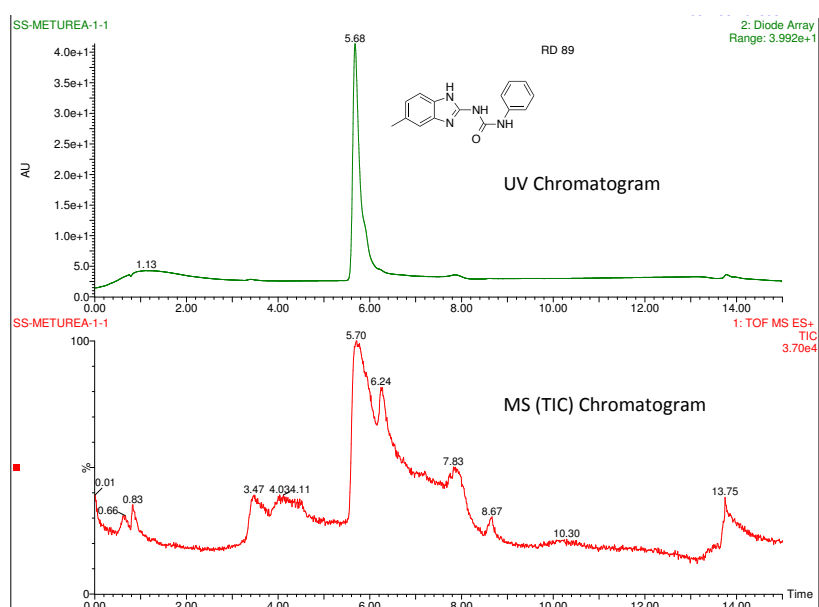


Figure 24. Liquid chromatogram for 1-(5-methyl-1H-benzo[d]imidazole-2-yl)-3-phenylurea

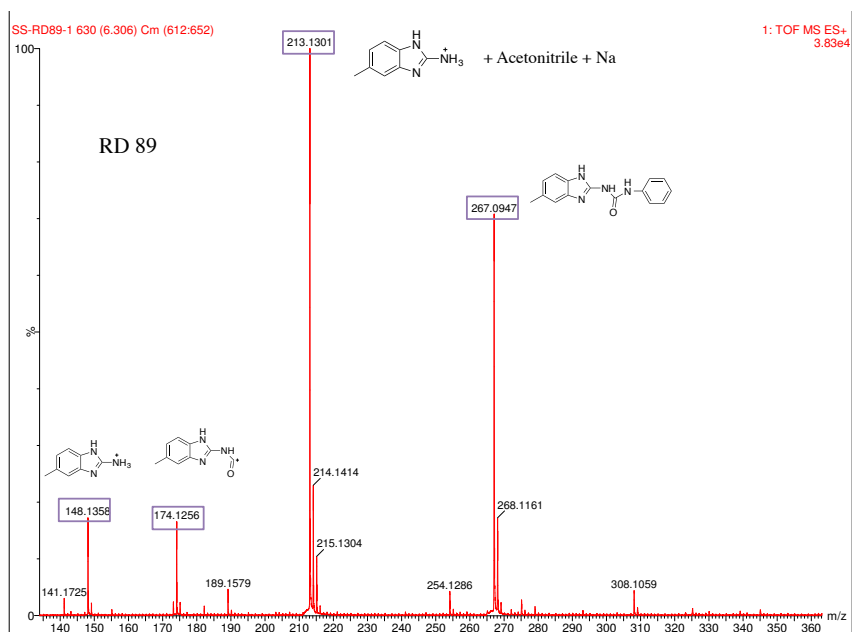


Figure 25. Mass Spectrum for 1-(5-methyl-1H-benzo[d]imidazole-2-yl)-3-phenylurea from peak at 5.68 minutes of TIC chromatogram on Figure 20.

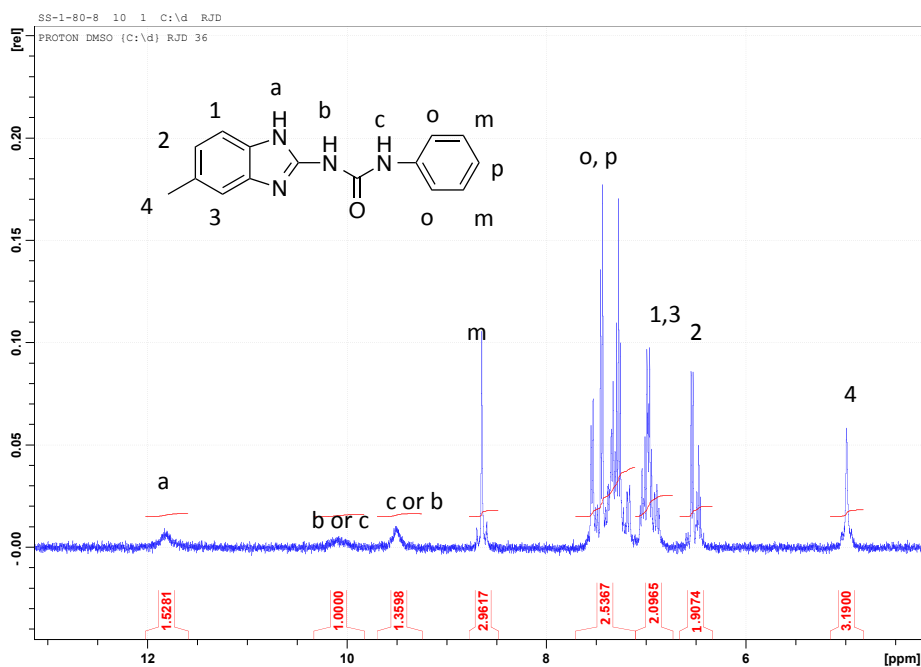


Figure 26. NMR spectrum for 1-(5-methyl-1H-benzo[d]imidazole-2-yl)-3-phenylurea. Proton a is in a more aromatic environment, thus it is more deshielded than protons b and c. On the other hand, protons b or c cannot be precisely assigned.

Biological evaluation of the p53 reactivation process

Biological assays are designed with the purpose of testing the biological activity of compounds towards a specific targeted disease. In the case of p53, the goal is to design assays that can test the reactivation of mutant p53 in cancer cells. To determine if a compound reactivates mutant p53 in human tumor cells, a buffered solution of a compound is placed in a culture of growing p53 mutant tumor cells (DLD1 colon cancer and SF295 glioblastoma brain cancer) and incubated for 18 hr. The cells are lysed and the cellular proteins are separated by gel electrophoresis and identified using a Western blot procedure. If proteins expressed by p53 are present, then the mutant p53 was reactivated. We follow the production of p21. When p53 is reactivated in these tumor cells, apoptosis should occur. By measuring the concentration of compound that kills half of the tumor cells, we get the cell-kill EC50. More potent compounds will have a reduced cell-kill EC50s. Off-target toxicity can be determined by also obtaining the cell-kill EC50 for a p53 null cell (H1299 cells). A generally nontoxic compound should have no effect on the cell containing no p53. Off-target toxicity is expressed as a therapeutic index, TI, as determined by formula 1 shown below (Muller, 2012).

$$TI = \frac{EC_{50}^{nullcell}}{EC_{50}^{tumorcell}} \quad (1)$$

Phase I *In vitro* Metabolism

Solutions

1) 898 μ L Assay Buffer. A 100 mL stock solution was prepared (100 mM Trizma, pH=7.4, 3 mM $MgCl_2$) using 10 mL of Trizma (T2663-1L, 1.0 M) and 0.061 g $MgCl_2 \cdot 6H_2O$, which was empirically found to enhance the microsomal drug-metabolizing enzyme systems directly since it gave a better results suggesting that the microsomes are more active in presence of magnesium ion (Marvin, 1970). HCl (0.100 M) used to adjust pH.

2) 25 μ L Microsomal Protein. 25 μ L of 0.5 mg/mL microsomal protein (purchased as 20 mg/mL, or 10 mg/0.5 mL; MX008061, pooled male, 10 mg/\$190 was used as is. BioreclamationIVT, 410-455-1242). The 10 mg/0.5 mL commercial material was divided into 20 plastic 1.5 mL microcentrifuge vials containing 25 μ L each. Stored vials in $-80^\circ C$ freezer or in liquid nitrogen Dewar.

3) 2 μ L Substrate Solution. 1 mL solution (25 μ M) was made using 1.3 mg in 1.0 mL acetonitrile, methanol, or DMSO. Latter is preferred.

4) 75 μ L NADPH. A fresh solution was made for each run. The 50 mg commercial sample (N1630-50mg, \$115) was divided into 50 plastic 1.5 mL microcentrifuge vials containing 1.0 mg each. 100 μ L of assay buffer was added to a vial for each run to obtain 1.0 mM. The total volume for each microsomal incubation tube was 1 mL.

Procedure

Incubations were performed in 16x100 mm glass culture tubes placed in a reciprocating water bath, set at 37°C. A microsomal vial (one per compound) was allowed to warm to ice bath temperature and then the 898 µL of assay buffer (1) was added. The mix was added to the tube. The substrate solution (3) was added to the mixture, which was vortexed to mix and then pre-incubated for 5 minutes at 37°C in the water bath. The reaction was initiated by addition of the NADPH solution (4). Three aliquots of 0.30 mL were removed at 15, 30, and 60 minutes. A zero point was set up by adding everything except for the microsomes (to account for the volume, 25 µL of assay buffer were added). Two aliquots of 0.30 mL were removed, one as soon as components are mixed and another at 60 minutes.

Treatment of each aliquot

0.5 mL acetonitrile were added as soon as each aliquot was taken, vortexed, transferred to microcentrifuge tube, and centrifuged at 13,000 rpm, 16,000 rcf (centrifugal force) for 3 minutes. 0.5 mL of the supernatant were then transferred to a clean LC/MS vial and analyzed by LC/MS.

Compound Concentration Calculation

All samples were quantitatively analyzed by LC/MS on an Agilent 1100 series HPLC and recorded on a Waters TOF, Micromass-LCT using an Analytical Advantage ECHELON C18 column using the following gradient described in **Table 5**.

15 minute run		
Analytical Echelon C18, 100X4.6 mm		
Water acetonitrile		
Flow 1.5 mL/min		
Time	%Aq	%B
0.0	70	30
1.0	70	30
8.0	30	70
9.0	30	70
11.0	20	80
12.0	15	85
13.0	70	30

Table 5. LC/MS 15 minutes run conditions

To determine the relative concentration of compounds using MS analysis, the molecular weight peak was searched for in the MS TIC (total ion current) liquid chromatogram. Integration of parent compound peak areas vs. time gives the raw metabolic rate.

Identification of Metabolites

To identify the metabolites for every RD compound synthesized and studied in Doll's Lab, the following procedure was followed:

1. The original MS TIC chromatogram does not provide useful information since the solution contains only traces of microsomes, NADPH, the compound, and the metabolites. Thus, relevant information cannot be derived from it directly.

An example of the original MS TIC is shown in **Figure 27**.

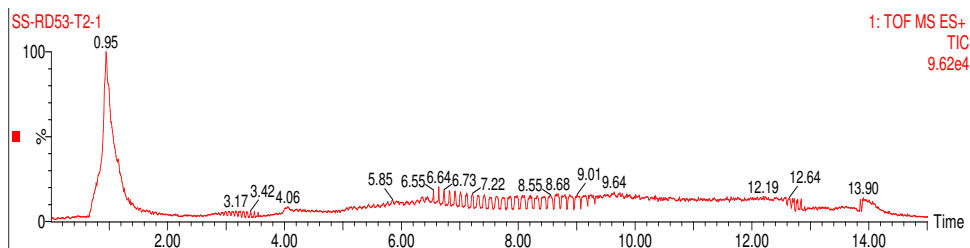


Figure 27. Full MS TIC chromatogram for Amide-H (RD 53) resulting from the microsomal assay.

- To retrieve useful information from this TOF MS chromatogram, the parent peak is followed by searching for its correspondent molecular weight plus 1 (MW+1), as shown in **Figure 28**.

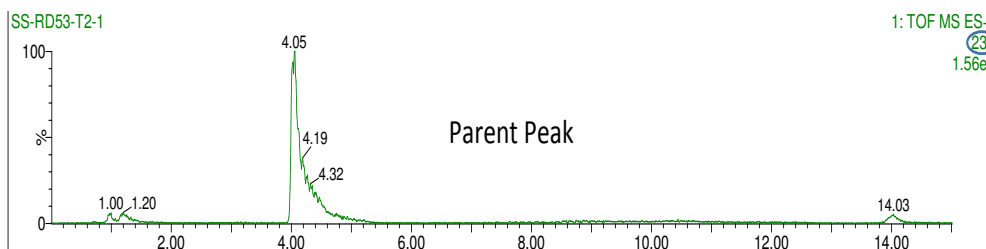


Figure 28. Extracted ion chromatogram for parent peak (MW+1=238) for Amide-H (RD 53) extracted from MS TIC chromatogram shown in **Figure 27**.

- To identify the metabolites, peaks corresponding to the molecular weight plus a hydroxyl (MW+16) and derivatives (MW+32, 64, etc.) were extracted from the original chromatogram as depicted in **Figure 29**. The ions comprising the TIC chromatographic peak can then be determined, allowing the assignment of structures to the ions.

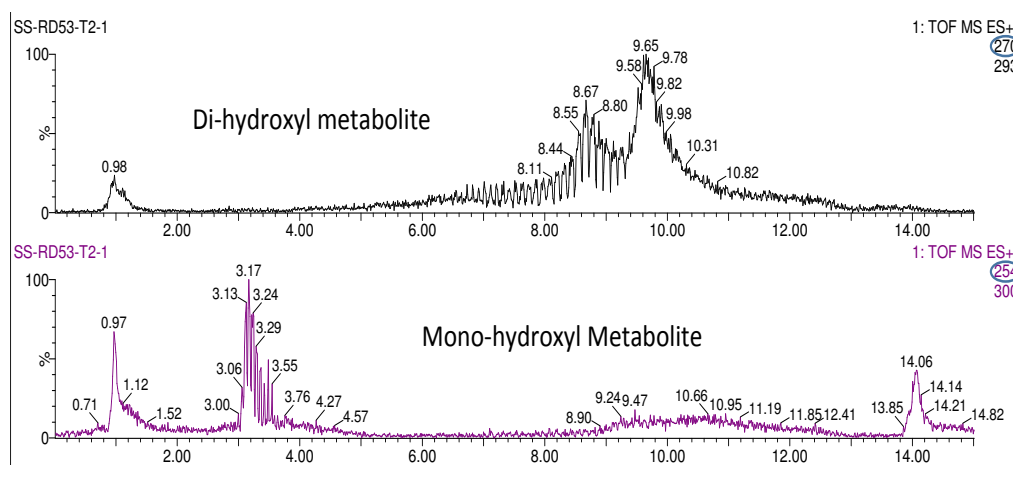


Figure 29. Extracted ion chromatogram for mono (MW+16=254) and di-hydroxyl (MW+32=270) metabolites peaks for Amide-H (RD 53) extracted from MS TIC chromatogram shown in **Figure 27**.

Metabolic Rate and Intrinsic Clearance Calculations

All integrated peak areas for the parent molecular ions peak obtained by LC/MS were normalized to natural logarithm of percent remaining of parent compound. A scatter plot of $\ln[\% \text{ remaining compound}]$ versus time was plotted using Excel, giving a downward sloping line. Half-life calculations were obtained using the slope of the line and equation (2).

$$t_{1/2} = \frac{\ln(2)}{-\text{slope} \ln(\% \text{ remaining drug})} \quad (2)$$

Since each experiment was performed in triplicate, error bars were obtained for each data point. The error bars utilized were obtained by the standard error, calculating the standard error of the mean corresponding to each data point. The standard error is calculated by dividing the standard deviation by the square root of number of measurements that make up the mean (often represented by N). In this case, 3 measurements were made (N = 3) so the standard deviation was divided by the square

root of 3, as shown in equation (3). With the standard errors calculated for each concentration at each data point, **Y Error Bars** were introduced by entering the **Error amount**, as the error bar method in Excel.

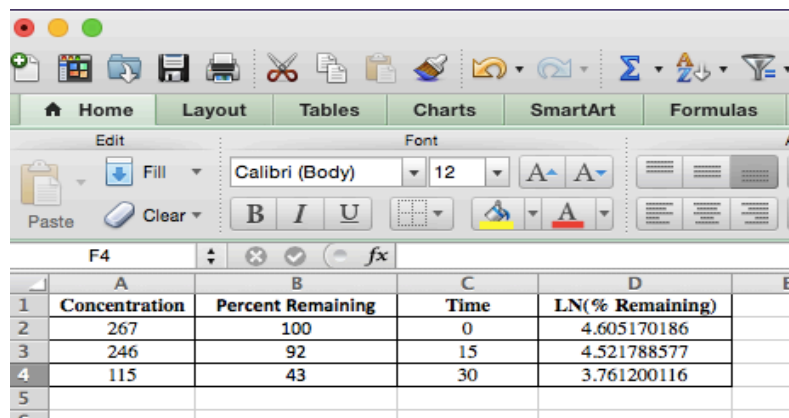
$$SE_{\bar{x}} = \frac{s}{\sqrt{n}} \quad (3)$$

Using the obtained value of $t_{1/2}$, the *in vitro* intrinsic clearance was calculated according to equation (4).

$$Cl_{int} = \frac{\ln(2)}{t_{1/2}} * 0.5 \frac{mL}{mg_{protein}} * \frac{1000 \mu L}{1 mL} \quad (4)$$

The procedure to enter the data on Mac Excel 2011 and graphing was done by the following process:

1. The data was enter in the cells of an Excel spreadsheet as shown in **Figure 30**



The screenshot shows the Mac Excel 2011 interface. The ribbon includes Home, Layout, Tables, Charts, SmartArt, and Formulas. The Font section is visible, showing Calibri (Body) font, size 12, and bold, italic, and underline options. The spreadsheet data is as follows:

	A	B	C	D	E
1	Concentration	Percent Remaining	Time	LN(% Remaining)	
2	267	100	0	4.605170186	
3	246	92	15	4.521788577	
4	115	43	30	3.761200116	
5					

Figure 30. Inserting data in cells of an Excel spreadsheet for Mac

2. Used the mouse to highlight the block of cells containing the data, and then clicked Insert: Chart. For Mac Excel 2011, the chart type desired was “marked scatter”, as shown in **Figure 31**.

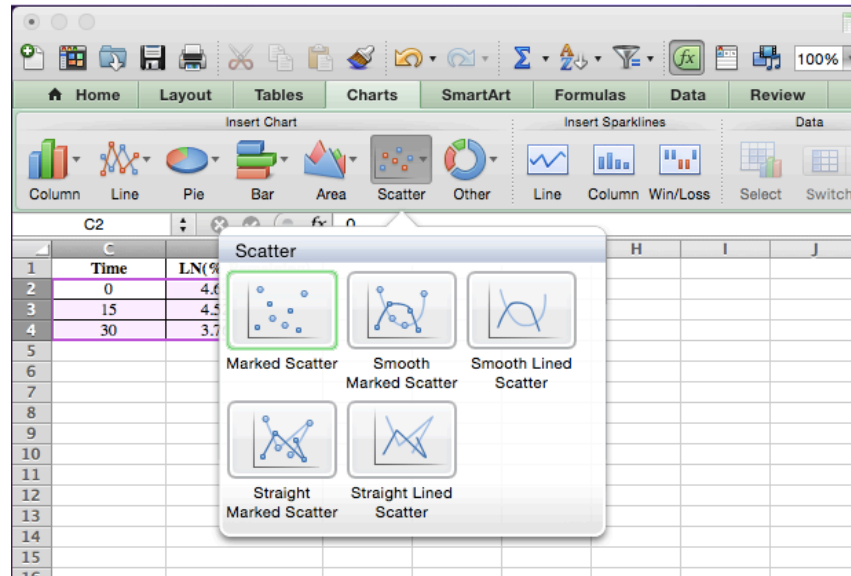


Figure 31. Inserting a straight marked scatter plot for the data points selected.

- Excel automatically generates a draft of the chart and pastes it into the worksheet, as shown in **Figure 32**.

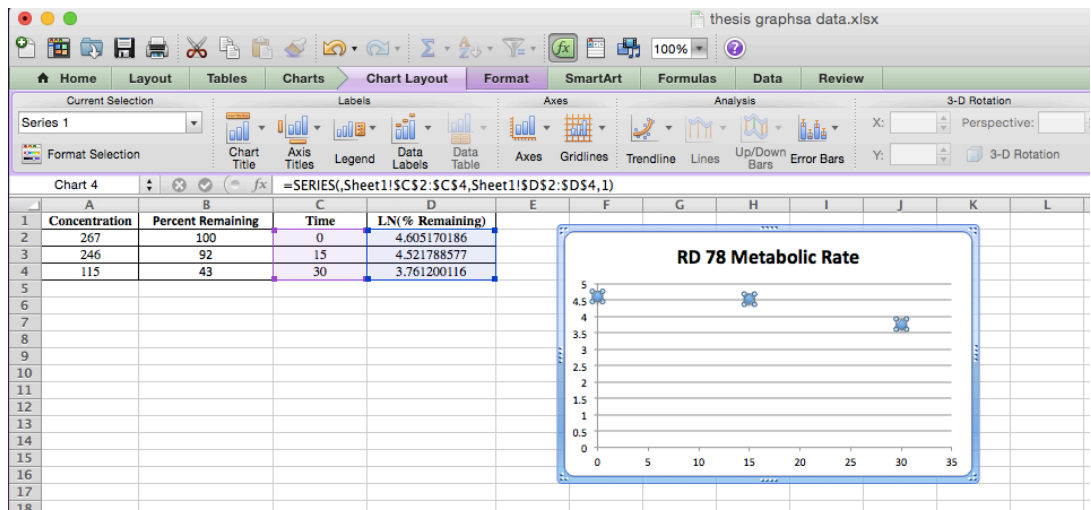


Figure 32. Automatically generated graph from Excel 2011

- To add labels and title, clicked on the “Chart Layout” tab, which brings up the chart format options. To start with, clicked on the tab called “Axis Titles,” where

the labels for the horizontal (X) axis and the vertical (Y) axis can be changed.

Added a chart title using the tab labeled “Chart Title”. See **Figure 33**.

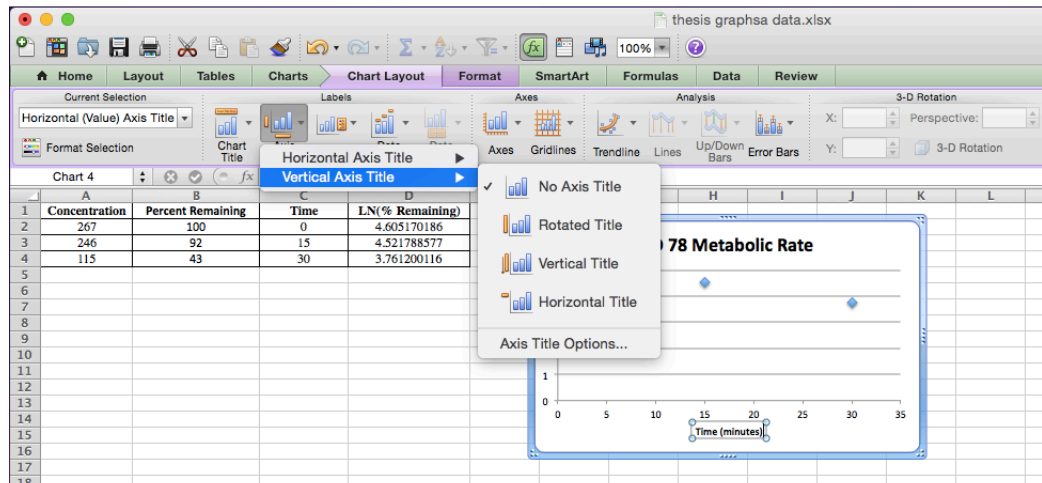


Figure 33. Labeling horizontal and vertical axis, and introducing titles to the automatically generated graph from Excel 2011

- To add a trend line (including the line equation and R^2 value), first clicked on the data points to activate them. From the drop-down box under the Chart menu at the top of the screen, selected Add Trendline. From the menu on the left side, selected Options. Checked the boxes for "Display equation on chart" and "Display R-squared value on chart", as shown in **Figure 34**.

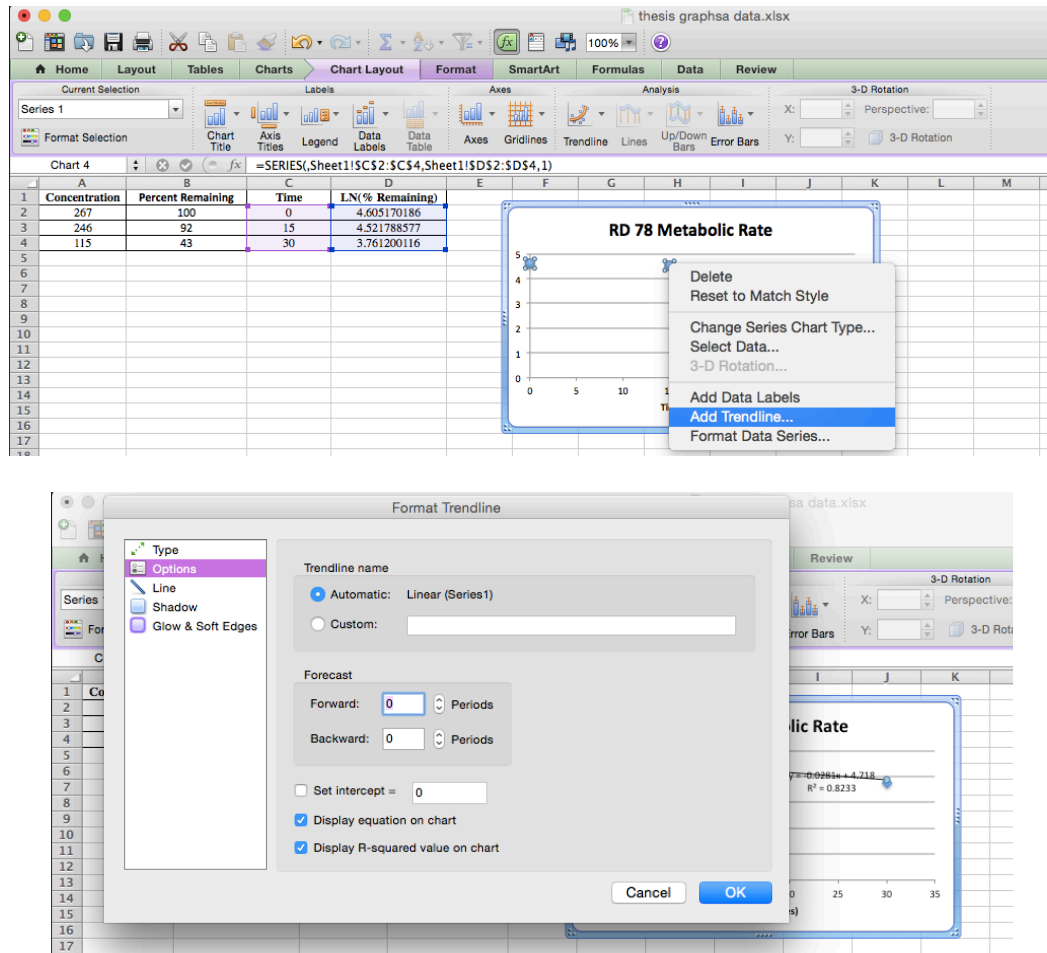


Figure 34. Inserting a linear trendline to the data points plotted.

RESULTS

Metabolic Rates and Intrinsic Clearances

The rate of the disappearance of the tested compound was plotted for the benzimidazole class of compounds, Urea-H (RD 38), Amide-H (RD 53), Amide-F (RD 78), Urea-F (RD 86), and Urea-M (RD 89) using the microsomal assay. From the slope of the linear trend, *in vitro* half-lives and *in vitro* intrinsic clearances were calculated using equation (1) on page 46.

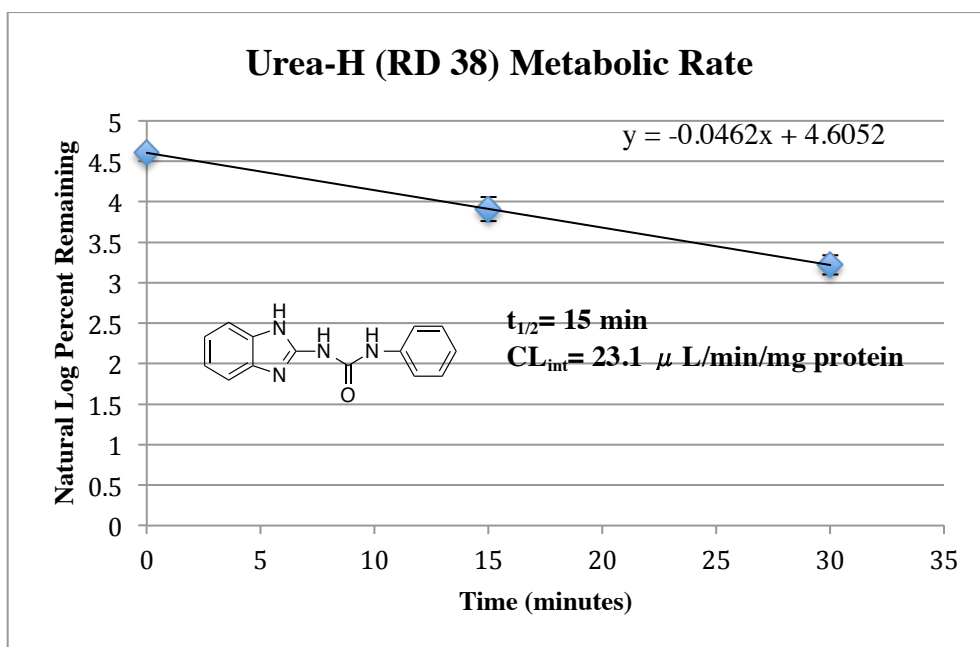


Figure 35. Natural logarithm of the percent remaining of concentration of Urea-H (RD 38) versus time in minutes. From the slope of the line equation, using equation (2) on page 46, we obtained the half-life of the compound $t_{1/2}$. Using equation (4) on page 47, we calculated the *in vitro* intrinsic clearance CL_{int} .

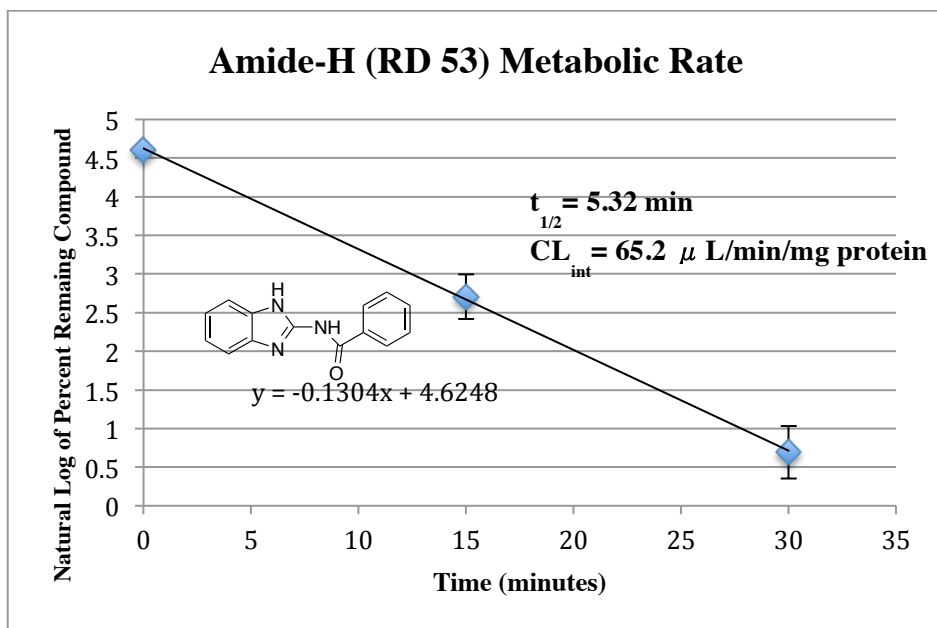


Figure 36. Natural logarithm of the percent remaining of concentration of Amide-H (RD 53) versus time in minutes. From the slope of the line equation, using equation (2) on page 46, we obtained the half-life of the compound $t_{1/2}$. Using equation (4) on page 47, we calculated the *in vitro* intrinsic clearance CL_{int} .

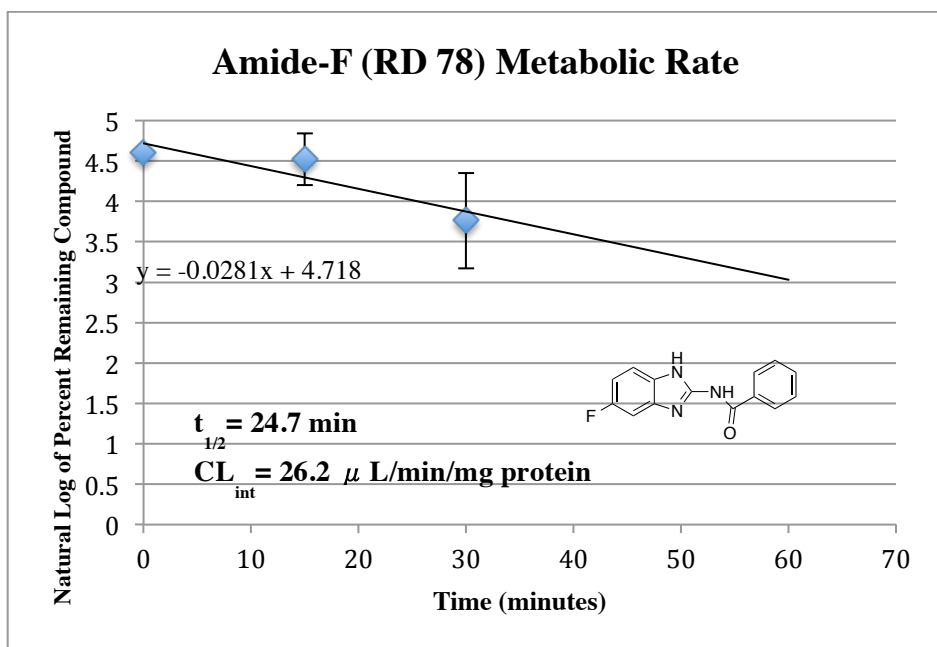


Figure 35. Natural logarithm of the percent remaining of concentration of Amide-F (RD 78) versus time in minutes. From the slope of the line equation, using equation (2) on page 46, we obtained the half-life of the compound $t_{1/2}$. Using equation (4) on page 47, we calculated the *in vitro* intrinsic clearance CL_{int} .

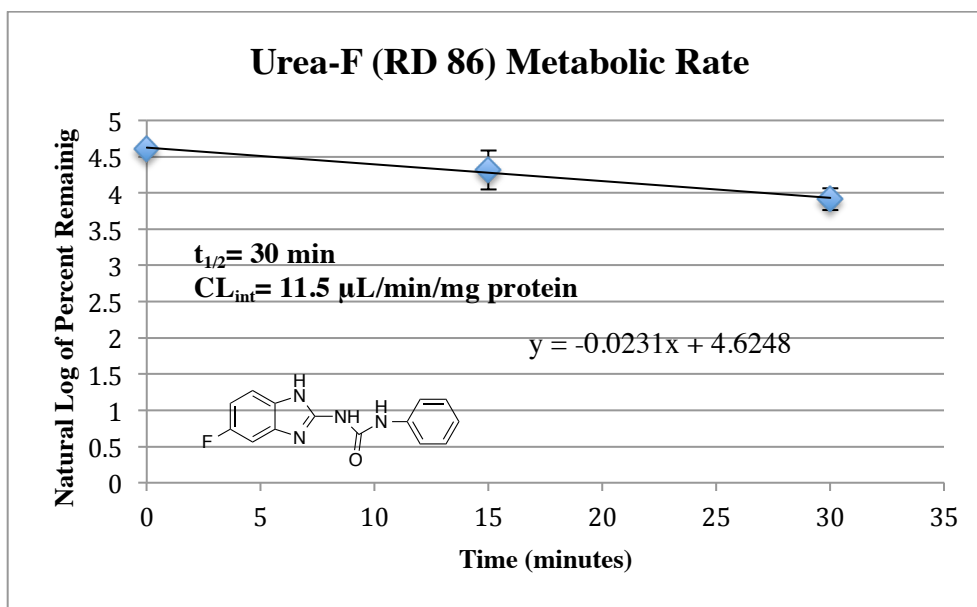


Figure 38. Natural logarithm of the percent remaining of concentration of Urea-F (RD 86) versus time in minutes. From the slope of the line equation, using equation (2) on page 46, we obtained the half-life of the compound $t_{1/2}$. Using equation (4) on page 47, we calculated the *in vitro* intrinsic clearance CL_{int} .

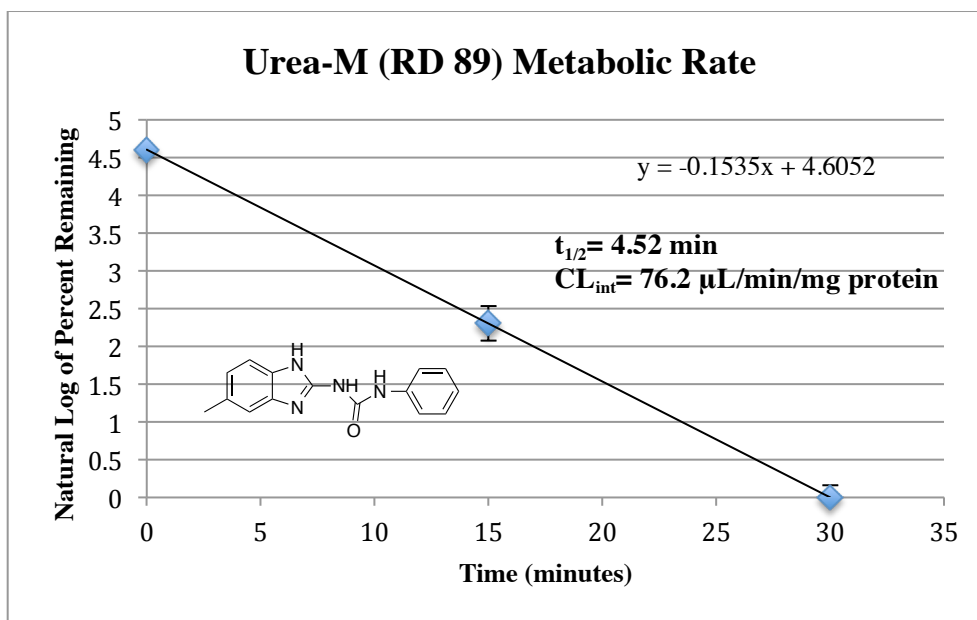


Figure 39. Natural logarithm of the percent remaining of concentration of Urea-M (RD 89) versus time in minutes. From the slope of the line equation, using equation (2) on page 46, we obtained the half-life of the compound $t_{1/2}$. Using equation (4) page 47, we calculated the *in vitro* intrinsic clearance CL_{int} .

Determination of Metabolites

From the LC/MS analysis, the metabolite structures were determined for Urea-H (RD 38), Amide-H (RD 53), Amide-F (RD 78), Urea-F (RD 86), and Urea-M (RD 89).

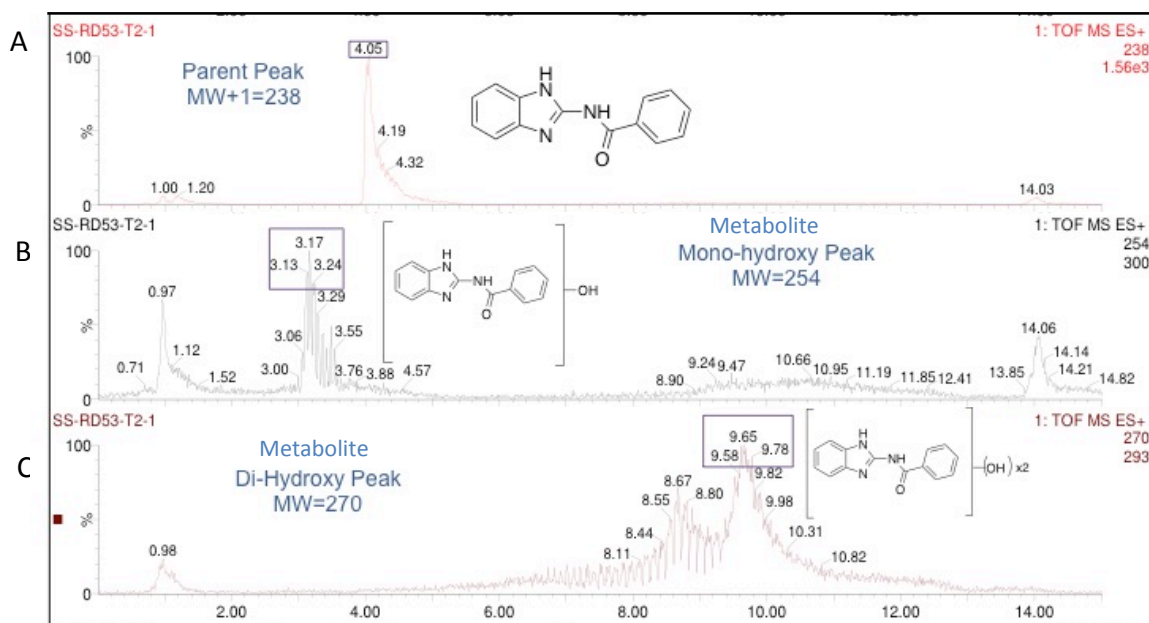


Figure 40. The liquid chromatograms for parent and metabolites of Amide-H (RD 53).

A. To identify the parent peak, the peak with the molecular weight corresponding to molecular weight plus one was searched following the analytical method described in figures 25-27. Parent peak for Amide-H (RD 53) showed at 4.05 minutes retention time. **B.** To identify the mono-hydroxylated metabolite, masses corresponding to the molecular weight plus 16 (monohydroxylation) were searched. The mono-hydroxylated metabolite showed a retention time corresponding to 3.17 minutes. **C.** To identify double hydroxylation metabolites, peaks for the molecular weight plus 32 (dihydroxylation) were searched. The di-hydroxy metabolite showed a retention times of 8.67 and 9.65 minutes.

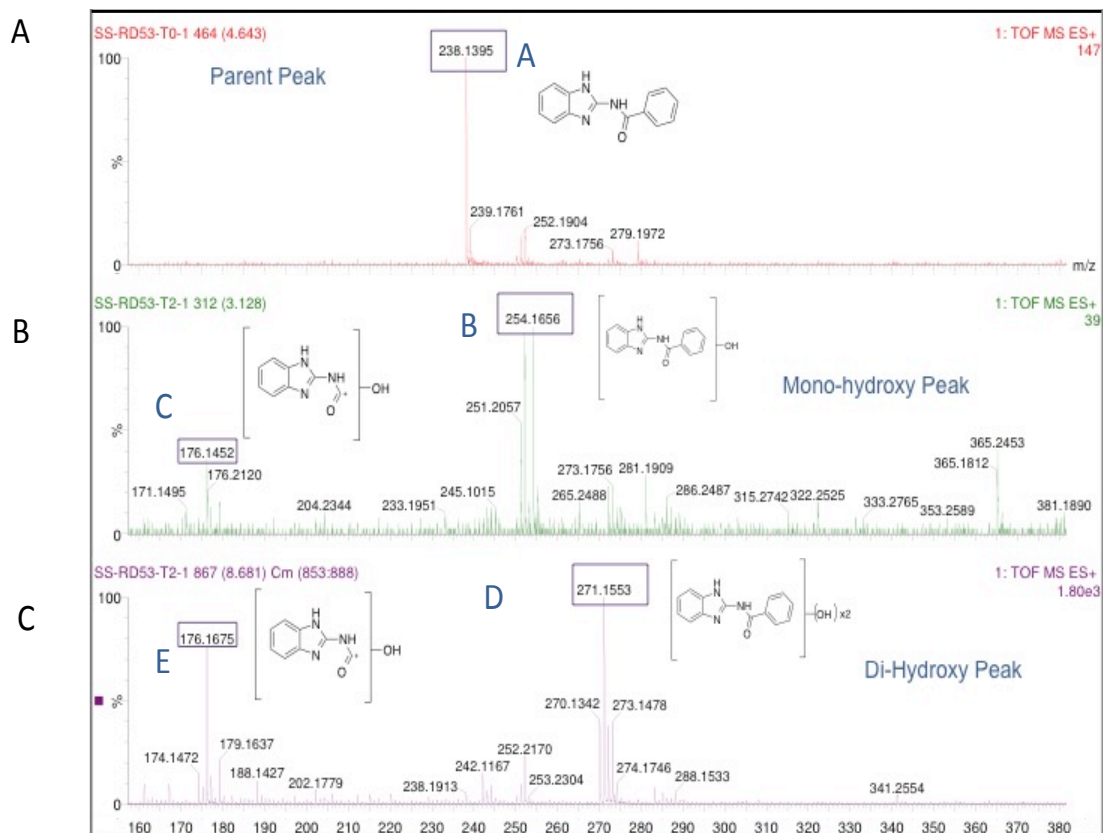


Figure 41. Mass Spectrum for peaks in Figure 40 – A, B and C.

A. The mass spectrum of the parent peak at 4.05 min **Figure 40-A** is shown above. Ion A corresponds to the molecular ion peak of Amide-H (RD 53) with 238.1 m/z. No significant fragments of Amide-H (RD 53) were observed under these conditions. **B.** For the metabolite peak at 3.17 min in **Figure 40-B**, ion B corresponds to the molecular ion peak and showed the expected molecular weight of 254.2 m/z. One relevant hydroxylated fragment ion is identified for Amide-H (RD 53) mono hydroxylated metabolite under these conditions. Ion C corresponds to the molecular weight of 176.1 m/z. **C.** For the metabolite peaks at 8.67 and 9.65 min in **Figure 40-C**, ion D corresponds to the molecular ion peak and showed a molecular weight of 271.2, corresponding to double hydroxylation. One relevant fragment is identified under these conditions for Amide-H (RD 53) double hydroxylated metabolite. Ion E corresponds to a mono-hydroxylated fragment with a molecular weight of 176.2 m/z.

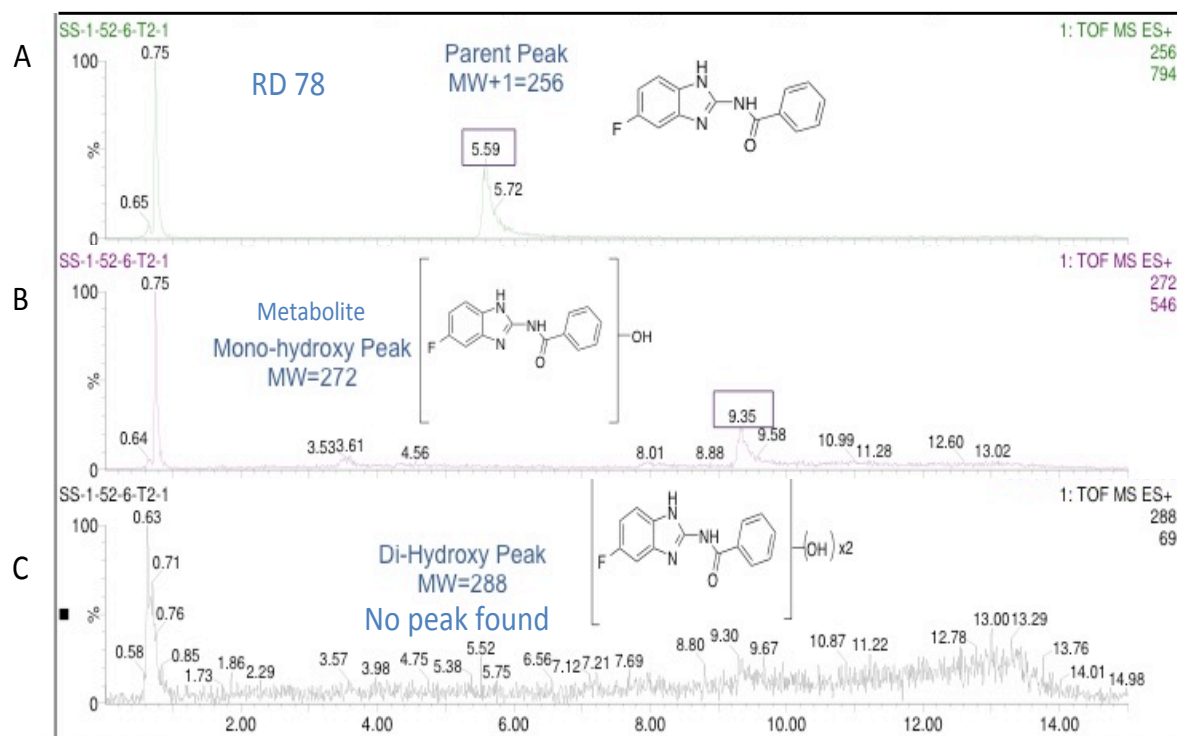


Figure 42. The liquid chromatograms for parent and metabolites of Amide-F (RD 78).

A. To identify the parent peak, the peak with the molecular weight corresponding to molecular weight plus one was searched following the analytical method described in 25-27. Parent peak for Amide-F (RD 78) showed at 5.59 minutes retention time. **B.** To identify the mono-hydroxylated metabolite, masses corresponding to the molecular weight plus 16 (monohydroxylation) were searched. The mono-hydroxylated metabolite showed a retention time corresponding to 9.35 minutes. **C.** To identify double hydroxylation metabolites, peaks for the molecular weight plus 32 (dihydroxylation) were searched. No peaks were identified for double hydroxylation metabolites.

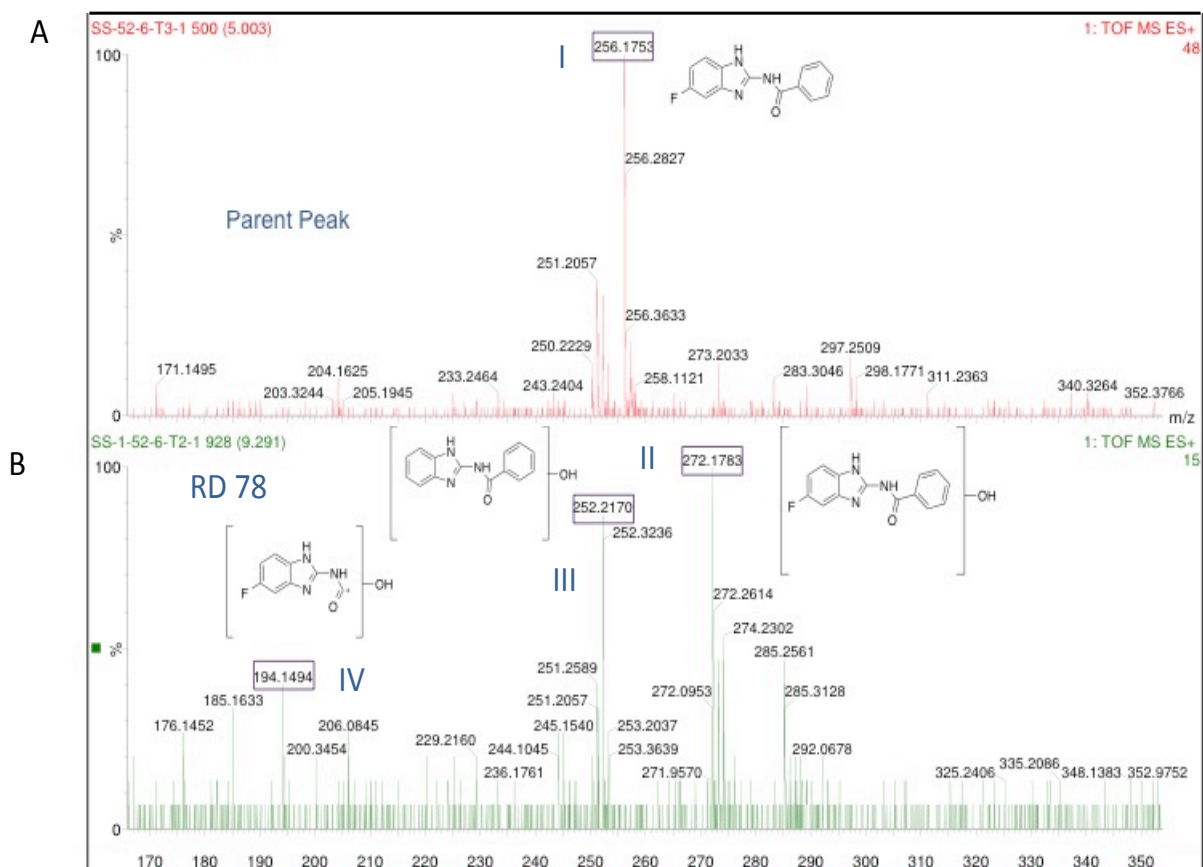


Figure 43. Mass Spectrum for peaks in Figure 42 - A and B.

- A.** The mass spectrum of the parent peak at 5.59 min **Figure 42-A** is shown above. Ion I corresponds to the molecular ion peak of Amide-F (RD 78) with 256.2 m/z. No significant fragments of Amide-F (RD 78) were observed under these conditions. **B.** For the metabolite peak at 9.35 min in **Figure 42-B**, ion II corresponds to the molecular ion peak and showed the expected molecular weight of 272 m/z. Two relevant hydroxylated fragment ions are identified. Ion III corresponds to the molecular weight of 252.2 m/z. Ion IV corresponds to the fragment of molecular weight 194 m/z.

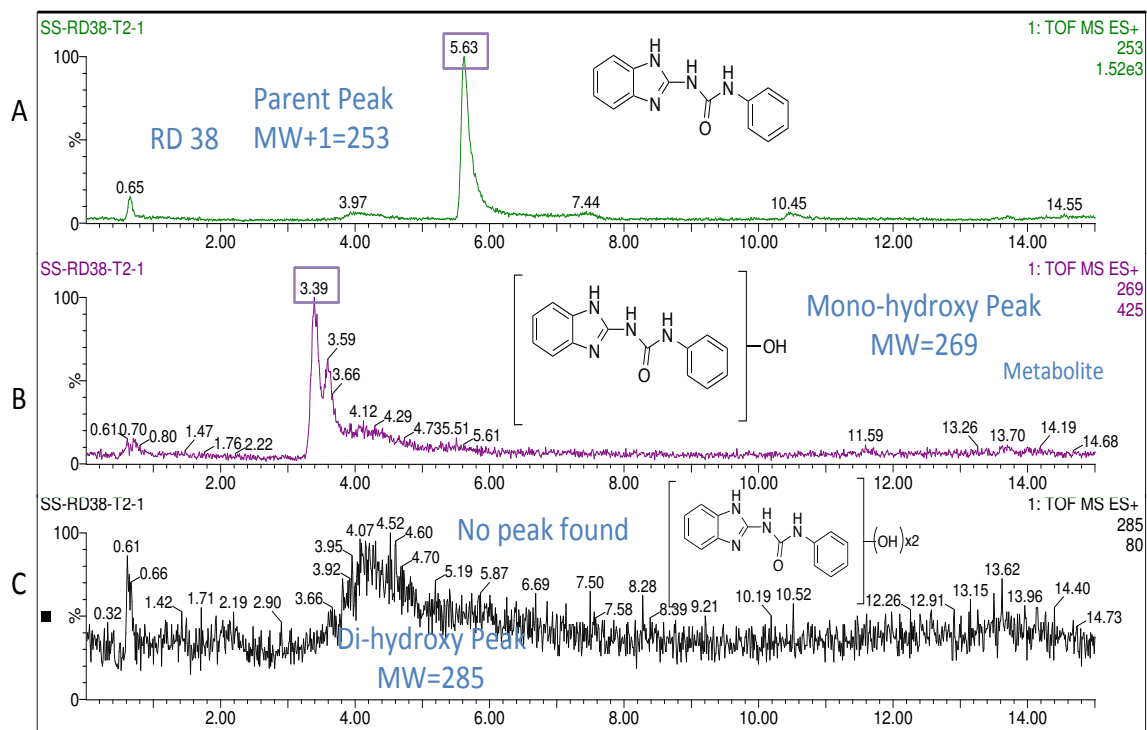


Figure 44. The liquid chromatograms for parent and metabolites of Urea-H (RD 38).

A. To identify the parent peak, the peak with the molecular weight corresponding to molecular weight plus one was searched following the analytical method described in figures 25-27. Parent peak for Urea-H (RD 38) showed at 5.63 minutes retention time. **B.** To identify the mono-hydroxylated metabolite, masses corresponding to the molecular weight plus 16 (monohydroxylation) were searched. The mono-hydroxylated metabolite showed a retention time corresponding to 3.39 minutes. **C.** To identify double hydroxylation metabolites, peaks for the molecular weight plus 32 (dihydroxylation) were searched. No peaks were identified for double hydroxylation metabolites.

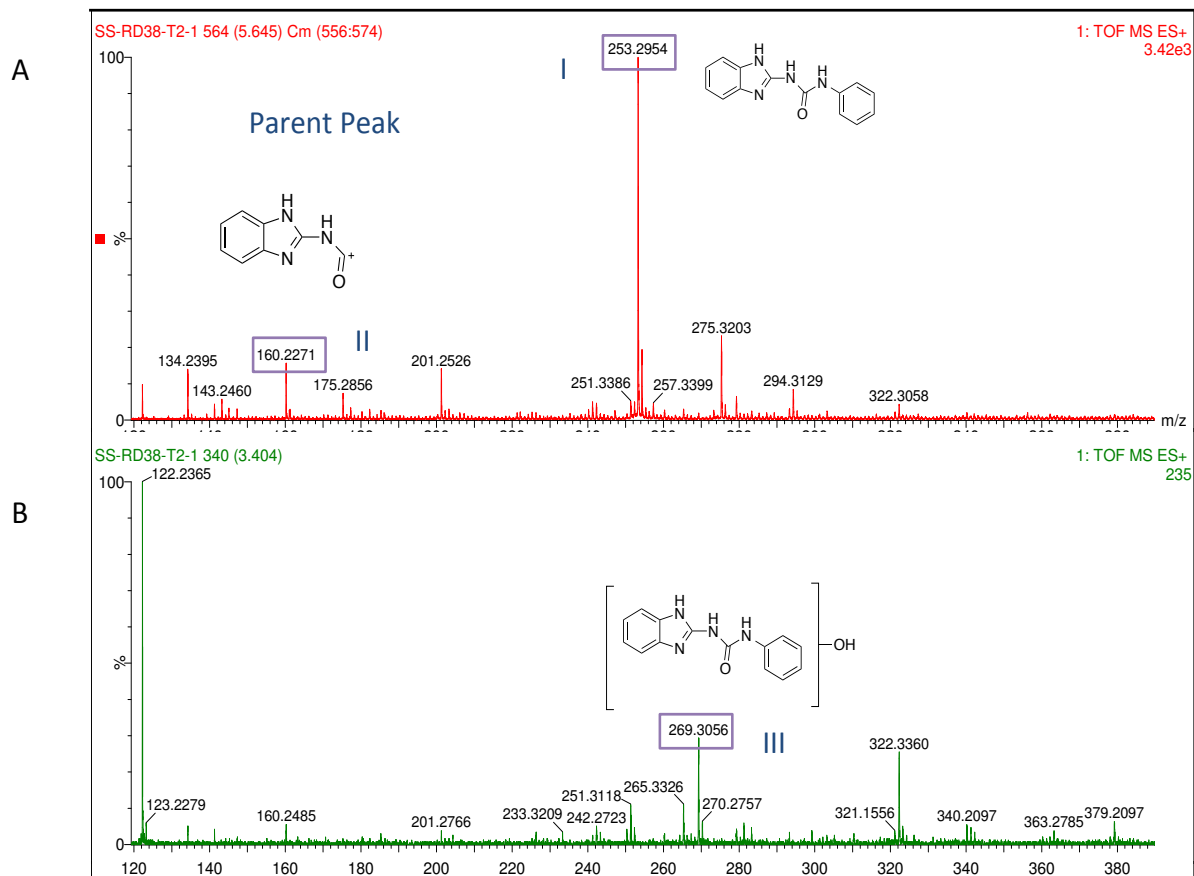


Figure 45. Mass Spectrum for peaks in Figure 44 - A and B.

A. The mass spectrum of the parent peak at 5.63 min **Figure 44-A** is shown above. Ion I corresponds to the molecular ion peak of Urea-H (RD 38) with 253.2954 m/z. One relevant ion was identified. Ion II corresponds to the molecular weight of 160.2271 m/z.

B. For the metabolite peak at 3.39 min in **Figure 44-B**, ion III corresponds to the molecular ion peak and showed the expected molecular weight of 269.3065 m/z. No relevant hydroxylated fragment ions were observed under these conditions.

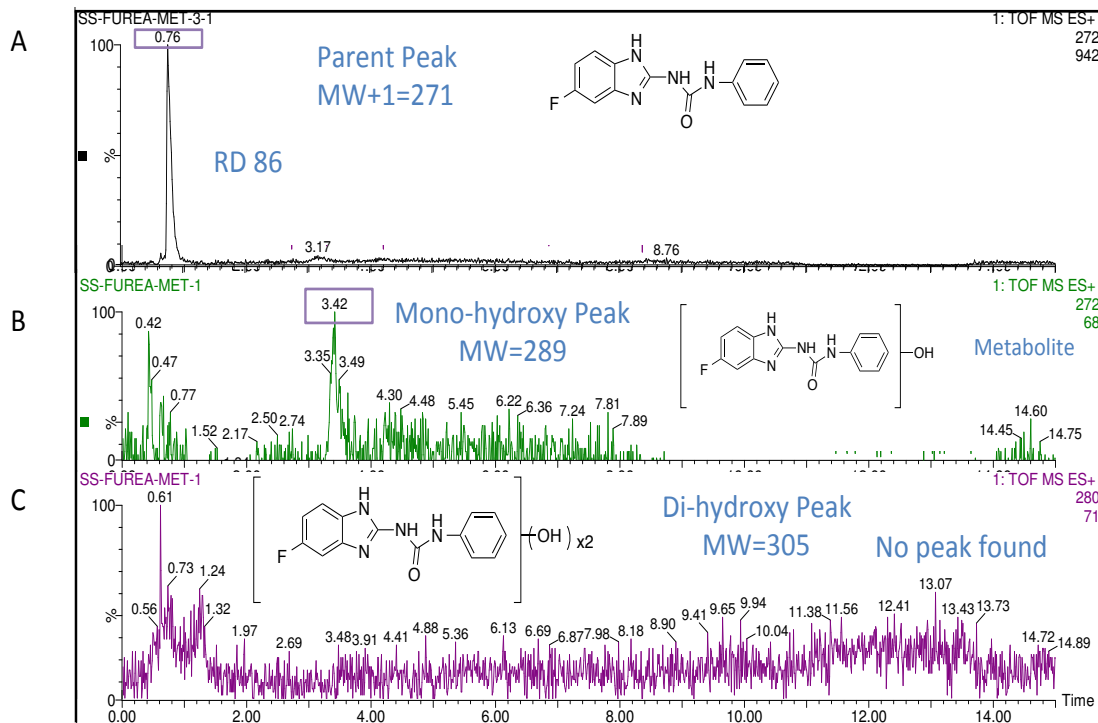


Figure 46. The liquid chromatograms for parent and metabolites of Urea-F (RD 86).

A. To identify the parent peak, the peak with the molecular weight corresponding to molecular weight plus one was searched following the analytical method described in figures 25-27. Parent peak for Urea-F (RD 86) showed at 0.76 minutes retention time. **B.** To identify the mono-hydroxylated metabolite, masses corresponding to the molecular weight plus 16 (monohydroxylation) were searched. The mono-hydroxylated metabolite showed a retention time corresponding to 3.42 minutes. **C.** To identify double hydroxylation metabolites, peaks for the molecular weight plus 32 (dihydroxylation) were searched. No peaks were identified for double hydroxylation metabolites.

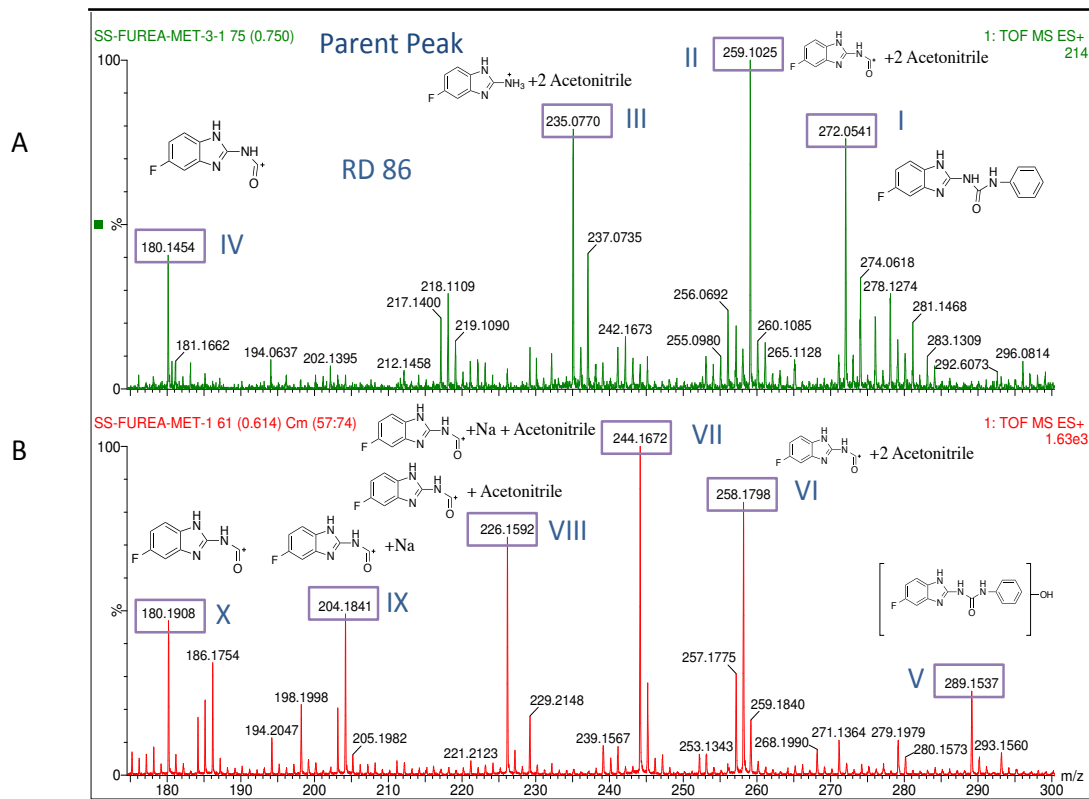


Figure 47. Mass Spectrum for peaks in Figure 46 - A and B.

A. The mass spectrum of the parent peak at 0.76 min **Figure 46-A** is shown above. Ion I corresponds to the molecular ion peak of Urea-F (RD 86) with 272.0541 m/z. Three relevant ions were identified. Ion II corresponds to the molecular weight of 259.1025 m/z; ion III corresponds to the molecular weight of 235.0770 m/z; and ion IV corresponds to the molecular weight of 180.1454 m/z. **B.** For the metabolite peak at 3.42 min in **Figure 46-B**, ion V corresponds to the molecular ion peak and showed the expected molecular weight of 289.1537 m/z. No relevant hydroxylated fragment ions were observed under these conditions. Fragments ions VI, VII, VIII, XI, and X are non-hydroxylated ions of Urea-F (RD 86).

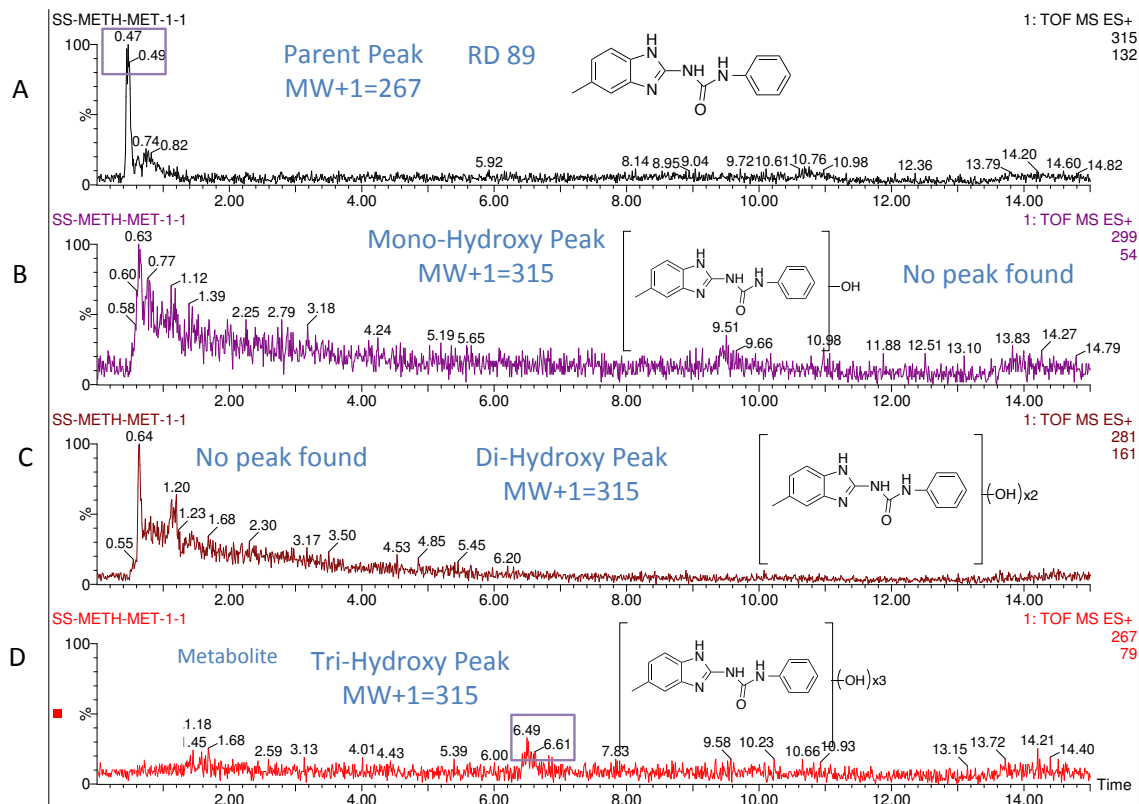


Figure 48. The liquid chromatograms for parent and metabolites of Urea-M (RD 89).

A. To identify the parent peak, the peak with the molecular weight corresponding to molecular weight plus one was searched following the analytical method described in figures 25-27. Parent peak for Urea-M (RD 89) showed at 0.47 minutes retention time. **B.** To identify the mono-hydroxylated metabolite, masses corresponding to the molecular weight plus 16 (monohydroxylation) were searched. No peaks were identified for single hydroxylation metabolites. **C.** To identify double hydroxylation metabolites, peaks for the molecular weight plus 32 (dihydroxylation) were searched. No peaks were identified for double hydroxylation metabolites. **D.** To identify the triple-hydroxylated metabolite, masses corresponding to the molecular weight plus 48 (trihydroxylation) were searched. The triple hydroxylation metabolite showed a retention time corresponding to 6.49 minutes.

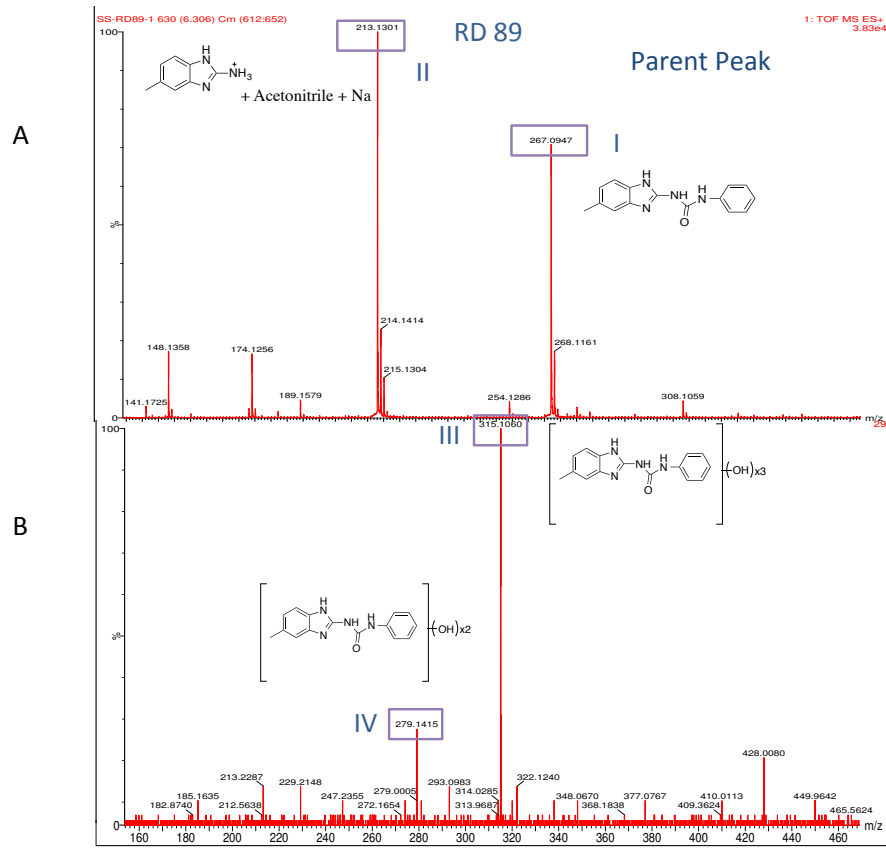


Figure 49. Mass Spectrum for peaks in Figure 48 - A and D.

A. The mass spectrum of the parent peak at 0.47 min **Figure 48-A** is shown above. Ion I corresponds to the molecular ion peak of Urea-M (RD 89) with 267.0947 m/z. One relevant ion was identified. Ion II corresponds to the molecular weight of 212.1301 m/z.

B. For the metabolite peak at 6.49 min in **Figure 48-B**, ion III corresponds to the molecular ion peak and showed the expected molecular weight of 315.1080 m/z. One relevant ion was identified. Ion IV corresponds to the molecular weight of 279.1416 m/z.

DISCUSSION

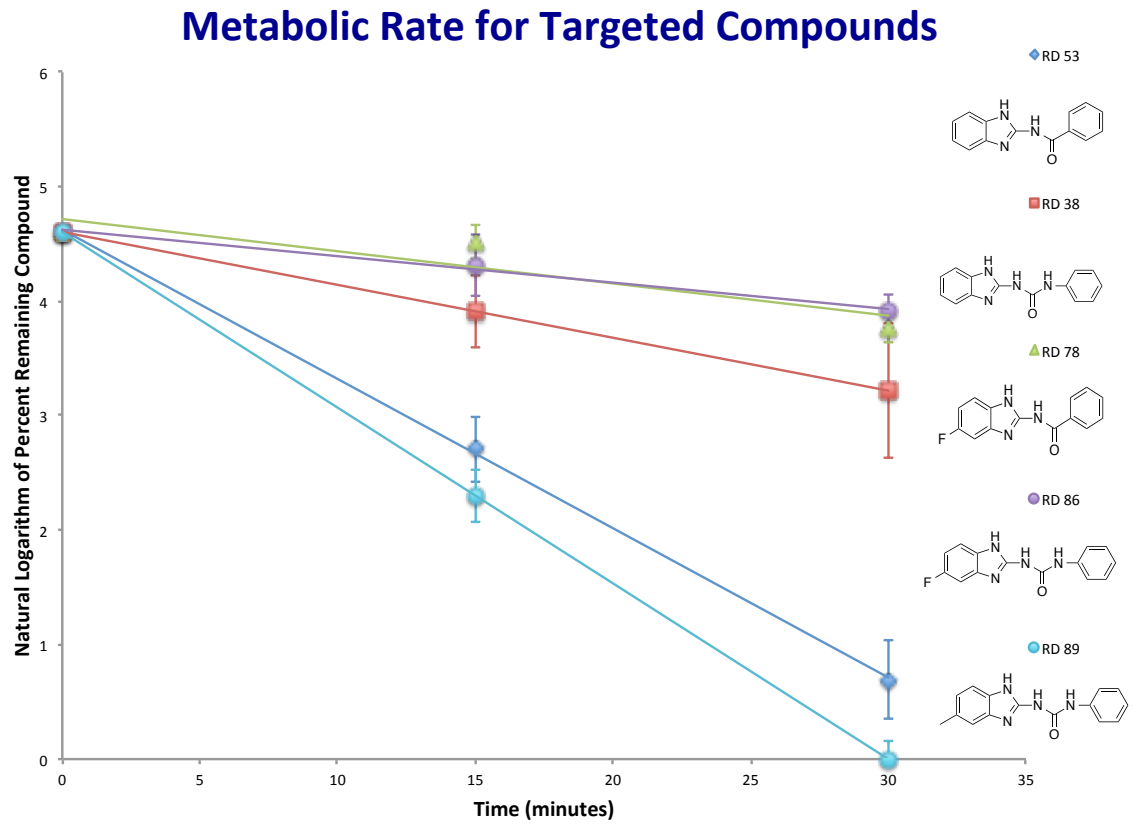


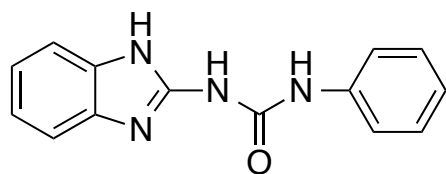
Figure 50. Metabolic rates for targeted compounds RD 53, RD 78, RD 38, RD 86, RD 89.

	Compound	CLogP	Half-life $t_{1/2}$	<i>In vitro</i> Intrinsic Clearance Cl_{int}	Metabolite	Ion Followed
Non-Fluorinated	Urea-H (RD 38) 	3.405	(15±2) min	23 $\mu\text{L}/\text{min mg protein}$		
	Amide-H (RD 53) 	2.901	(5.3±2.1) min	65 $\mu\text{L}/\text{min mg protein}$		
Fluorinated	Amide-F (RD 78) 	3.135	(25±2) min	26 $\mu\text{L}/\text{min mg protein}$		
	Urea-F (RD 83) 	3.650	(30±2) min	12 $\mu\text{L}/\text{min mg protein}$		
Methyl	Urea-M (RD 89) 	3.904	(4.5±1.5) min	76 $\mu\text{L}/\text{min mg protein}$		

Table 6. *In vitro* half-lives and intrinsic clearance, metabolites and active sites for RD's compounds.

Metabolism of RD Compound

Urea-H RD 38



RD 38 is a urea benzimidazole class of compound that undergoes single (M+16) hydroxylation by cytochrome p450 at the benzimidazole portion of the compound, as shown in **Figure 51**.

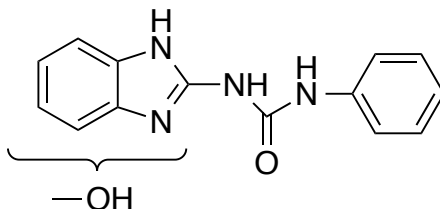
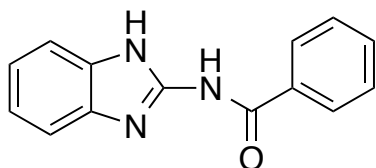


Figure 51. Diagram of the location of the hydroxyl group in the benzimidazole portion of the ring for the metabolite of Urea-H (RD 38).

The metabolic rate for this compound is $t_{1/2}=15$ minutes and it has *in vitro* intrinsic clearance of 23 $\mu\text{L}/\text{min mg protein}$.

Amide-H RD 53



RD 53 is an amide benzimidazole compound that undergoes double hydroxylation by cytochrome p450, as indicated by a molecular ion of $M+32$ in the mass spectrum (MS) on **Figure 40**. Mono-hydroxylation ($M+16$) was observed in the benzimidazole portion of the molecule, as shown in **Figure 41**. The second hydroxyl does not appear in the benzimidazole fragment in the MS, as shown in **Figure 41**. **Figure 52** shows the possible positions of the hydroxylation sites of the compound. RD 53 is rapidly metabolized, with a metabolic rate of $t_{1/2}=5$ minutes and an *in vitro* intrinsic clearance of 65 $\mu\text{L}/\text{min mg protein}$.

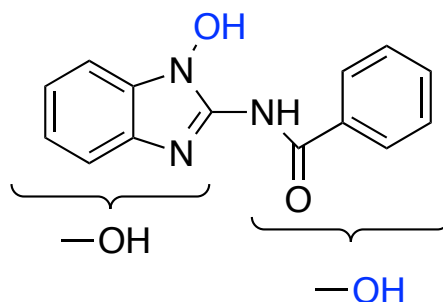
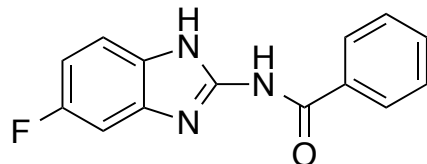


Figure 52. Possible positions of the two hydroxyl groups added after metabolism by cytochrome p450 on Amide-H (RD 53). The two blue $-OH$ groups correspond to possible locations of the second hydroxyl.

The metabolite with lower retention time shown in **Figure 40-B** – the metabolite that results from single (M+16) hydroxylation by cytochrome p450 – contains the hydroxyl group in the benzimidazole portion of the ring.

Amide-F RD 78



RD 78 is a fluorinated amide benzimidazole class of compound that undergoes single (M+16) hydroxylation by cytochrome p450 at the benzimidazole portion of the compound, as shown in **Figure 53**.

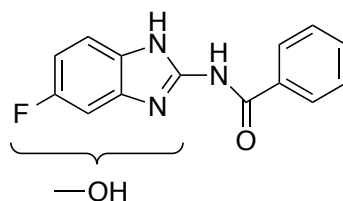
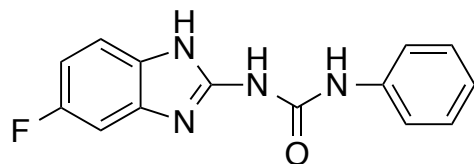


Figure 53. Diagram depicting the addition of the hydroxyl group at the benzimidazole portion of the ring in Amide-F (RD 78).

The mass spectral data shown in **Figure 43** indicates that the hydroxyl group is added to the benzimidazole portion of the ring. RD 78 was more metabolically stable compared to its analogous Amide-H (RD 53) by 5 folds, with a metabolic rate of $t_{1/2}=25$ minutes and an *in vitro* intrinsic clearance of 26 $\mu\text{L}/\text{min mg protein}$.

Urea-F RD 86



RD 86 corresponds to the fluorinated urea benzimidazole compound (Urea-F) and it undergoes single (M+16) hydroxylation by cytochrome p450 as shown by the parent ion of M+16 in the MS, as shown in **Figure 54**.

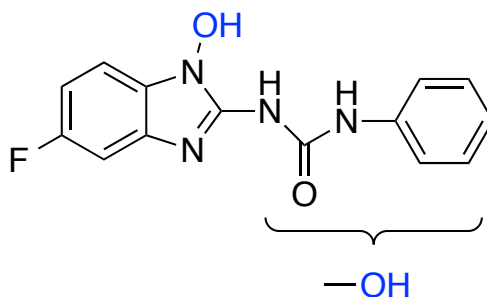
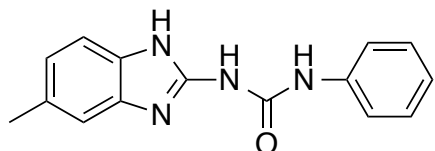


Figure 54. Diagram depicting the structure of the metabolite for Urea-F (RD 86).

As shown in **Figure 47**, the benzimidazole fragment ion does not show an OH (M+16). Urea-F is more metabolically stable than the lead structure Urea-H (RD 38), with a metabolic rate two folds slower of $t_{1/2}=30$ minutes and an *in vitro* intrinsic clearance of 12 $\mu\text{L}/\text{min mg protein}$.

Urea-M RD 89

RD 89 is a urea benzimidazole class of compound that has a methyl substituent at the 5-position of the benzimidazole ring, and it undergoes triple hydroxylation by cytochrome p450, as shown in **Figure 55**.

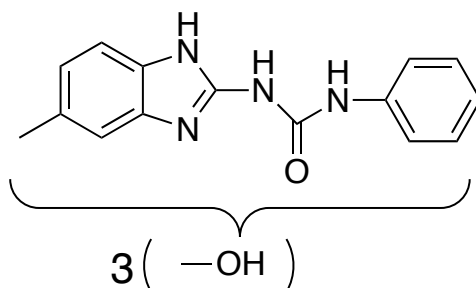


Figure 55. Diagram depicting the triple hydroxylation of Urea-M (RD 89).

As shown in **Figure 48**, no single (M+16) or double (M+32) hydroxylation was observed for RD 89, only a peak corresponding to triple (M+48) hydroxylation was observed for this compound. RD 89 was the least metabolically stable compound with a metabolic rate 3 folds faster than the lead structure Urea-H (RD 38) of $t_{1/2}$ =5 minutes and an *in vitro* intrinsic clearance of 76 $\mu\text{L}/\text{min mg protein}$.

Metabolic Data (Possible structures of metabolites)

Amides vs. Ureas

In vitro human metabolic data, displayed in **Table 6** on page 65, show that the benzimidazole class of compounds undergo single hydroxylation by cytochrome P450 enzymes at the benzimidazole portion of the ring with the exception of Amide-H (RD 53) and Urea-M (RD 89). Amide-H (RD 53) undergoes double hydroxylation and Urea-M (RD 89) undergoes triple hydroxylation by cytochrome p450.

Furthermore, before fluorination, urea benzimidazoles were observed to be more metabolically stable than amide benzimidazoles. As shown in **Table 6**, the metabolic rate of Amide-H (RD 53) was $t_{1/2}=5$ minutes whereas the metabolic rate for Urea-H (RD 38) was determined to be $t_{1/2}=15$ minutes. This 3 fold difference in the metabolic rates shows that urea benzimidazoles are associated with a lower *in vitro* intrinsic clearance, which could potentially lead to larger percent bioavailability if oral absorption is good. An increase in percent bioavailability is correlated to a decrease in metabolic rate for *in vivo* models; in terms of pharmacokinetics, a higher percent bioavailability suggests that a larger fraction of the compound will reach the systemic circulation (Griffin, 2009). A larger percent bioavailability allows for more orally administrated fraction of a drug to reach the systemic circulation. Hence, a slower metabolic rate and better oral absorption is directly related to a larger percent bioavailability. However, we have not yet evaluated membrane transport rates for crossing GI membranes associated with our compounds and cannot comment on oral absorption. Amide-H (RD 53) showed double hydroxylation (as seen in **Figure 40**) while Urea-H (RD 38) underwent single hydroxylation only (as

shown in **Figure 44**). Although the number of metabolites is not directly related to metabolic stability, it is a factor to take into consideration when thinking of the biological activity or toxicity of the metabolites. In the case of Amide-H (RD 53), these metabolites were identified by mass spectrometry (shown in **Figure 41**), where two distinct metabolites were observed for each molecular weights of mono-hydroxy (MW=254) and di-hydroxy (MW= 270). The mono-hydroxy metabolite was successfully located in the benzimidazole portion of the compound as shown in **Figure 41**. However, for the di-hydroxy metabolite, one hydroxyl group was successfully located at the benzimidazole ring; the second hydroxyl group cannot be precisely located under these conditions of mass spectral analysis. Two theories can explain this. The first one is that the second hydroxyl group for the double hydroxylation is located somewhere else in the molecule apart from the benzimidazole portion, for which case the hydroxyl is lost with the fragmentation of the molecule in the mass spectrometer, as shown in **Figure 56**.

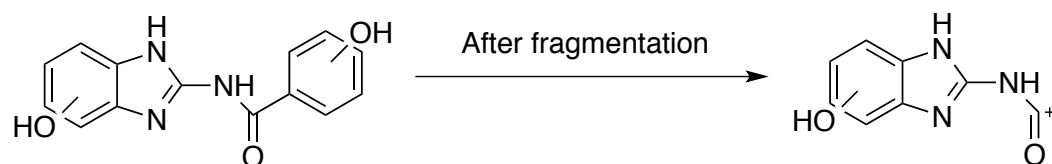


Figure 56. Diagram depicting the loss of one –OH group by fragmentation of Amide-H (RD 53) under MS conditions, yielding an ion with molecular weight corresponding to a mono-hydroxylated fragment.

The second hypothesis is that the second hydroxyl group is bonded with the –NH in the benzimidazole ring; hetero bonds like N-O are readily cleaved under mass spectra conditions, as shown in **Figure 57**, which explains why the fragment ion would not show the molecular weight corresponding for the ion + 32.

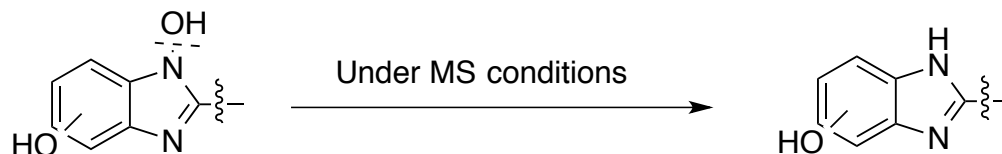


Figure 57. A diagram depicting cleavage of N-O hetero bond under MS conditions, yielding a molecular weight corresponding for a mono-hydroxylated Amide-H (RD 53). The ionization voltage could be lowered so the di-hydroxylated fragment may survive.

Fluorinated Compounds vs. Non-Fluorinated Compounds

For both amide and ureas, addition of fluorine as a substituent decreases the metabolic rate, which is seen in the half-lives of the compounds in **Table 6**. This is in accordance with the hypothesis and results shown in Nassar et al. 2004 where the authors observed an increased in percent bioavailability (%F) for an orally administrated drug after addition of fluorine. Furthermore, amongst the strategies presented in Di et al (2011), fluorination of lead structures at hydroxylation sites improve metabolic stability by decreasing the likelihood of hydroxylation at the site of metabolism. Thus, since the metabolic rate is related to metabolic stability, the decrease in metabolic rates upon fluorination observed for benzimidazole class of compounds indicates that these new compounds – Amide-H (RD 78) and Urea-F (RD 86) – are more metabolically stable than the lead structures Amide-H (RD 53) and Urea-H (RD 38).

In the case of Urea-F (RD 86), the metabolite hydroxyl group was not observed to be located at the benzimidazole portion of the ring by fragmentation in the mass spectrum. The absence of the hydroxyl in the fragment ions might be due to either of two factors. In the first case, the hydroxyl might be located in the phenyl group on the right side of the molecule and thus it is not observed in the mass spectrum, presumably

because that fragment it is not ionized. The other scenario is that the hydroxyl substituent is located at the –NH position of the benzimidazole ring; hetero-atomic bonds like N-O are easily cleaved under mass spectrum conditions.

Fluorination of Amides vs. Fluorination of Ureas

As mentioned above, the difference in terms of metabolic stability between non-substituted amides and ureas is around 3 fold, which indicates that ureas – in this case Urea-H (RD 38)– are considerably more metabolically stable than amides. However, after fluorination of compounds, as shown in **Table 6**, amides and ureas benzimidazoles have similar metabolic rates. With closer metabolic rates of $t_{1/2}=25$ minutes and $t_{1/2}=30$ minutes for amide and urea, respectively, fluorination of amide benzimidazole class of compounds have a greater impact in decreasing metabolic rates compared to urea benzimidazoles. Thus, fluorinated amides and fluorinated ureas are closer in metabolic stability than non-substituted molecules.

Effects of electron-donating groups

To further prove that an electron-withdrawing group at the metabolic site would decrease the rate of hydroxylation of compounds by cytochrome P450, addition of methyl (an electron donating group) as a substituent at the benzimidazole portion of the ring was synthesized to evaluate its metabolic profile. Urea-M (RD 89) showed a faster metabolic rate of $t_{1/2}=5$ minutes compared to $t_{1/2}=15$ minutes of Urea-H (RD 38), as shown in **Table 6**. This indicates that the new compound Urea-M (RD 89) is less metabolically stable than the lead structure Urea-H (RD 38), as metabolic stability is defined in terms of metabolic rates (Di, 2011).

Also, as shown in **Figure 48**, Urea-M (RD 89) undergoes triple hydroxylation by cytochrome P450. The effects of methyl as an electron-donating group not only speed up the hydroxylation by cytochrome P450, but also provide a new site of metabolism by hydroxylation at the methyl position, as shown in **Figure 58**.

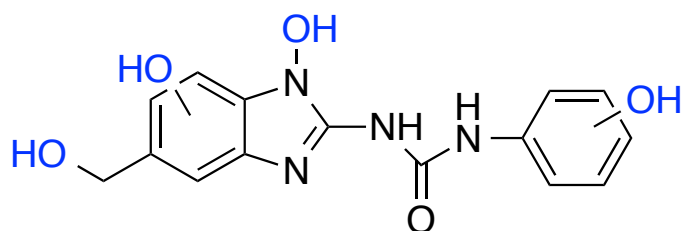


Figure 58. Diagram depicting the possible sites of hydroxylation by cytochrome p450, including the methyl position, the benzimidazole portion of the ring, and the phenyl portion of the compound. The blue hydroxyl groups represent the possible locations of the three –OH. The exact position of the three hydroxyl cannot be determined under these MS conditions since no fragmentation was observed.

However, only triple hydroxylation was identified by LC/MS analysis, as shown in **Figure 47** – no peaks were found for mono or double hydroxylation. In the mass spectrum analysis, triple hydroxylation was observed following the parent ion peak – no fragmentation was observed under the conditions of the LC/MS so the position of the hydroxyl groups could not be determined. An LC/MS/MS analysis, which causes additional fragmentation, can be performed in an attempt to locate the position of the hydroxyl groups in the metabolites.

LogP, CLogP and Lipophilicity

Structural changes not only affect metabolic stability of compounds; as part of drug discovery design process, the lipophilicity of the molecule also has to be considered and evaluated. Lipophilicity is relevant to the design of the drug because it determines if

the compound will be able to cross biological barriers like the gastro-intestinal track (GI membrane) and the blood brain barrier (BBB). Since the membrane permeability of a compound class is optimum at a particular lipophilicity window, determining the LogP of the compound, which is the logarithm of its partition coefficient, the ratio of solubility between n-octanol and water $\log(c_{\text{octanol}}/c_{\text{water}})$, would be useful (Di, 2011). CLogP is the calculated LogP, based on several verified algorithms. Thus, lower polarity (hydrophilicities) is related to high LogP values. A LogP window, based on structural class, is usually associated with a compound's ability to cross biological membranes. Addition of electron-donating or electron-withdrawing groups directly affects hydrophilicity as shown in **Table 6**, since structural changes cause variation in the values for CLogP. In **Figure 59**, the Gaussian distribution for CLogP of different marketed drugs is shown (Ghose, 2012). The majority of the marketed drugs have CLogP values between 2.5 and 4 logarithmic units. All of our compounds shown in **Table 6** fit into this CLogP window.

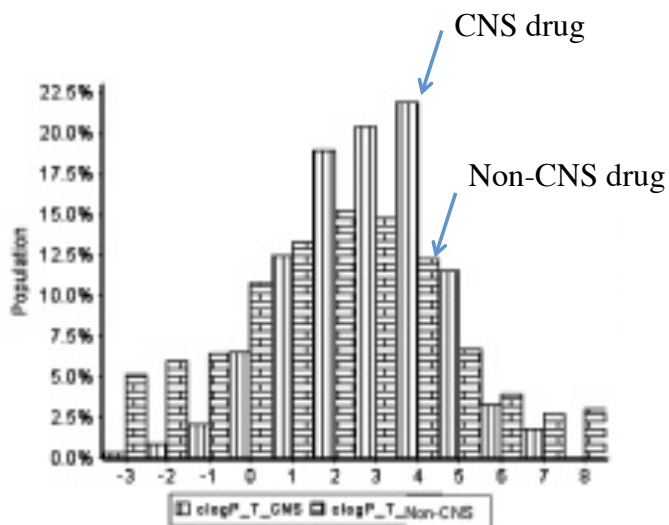


Figure 59. Distribution in a selection of marketed drugs (Ghose, 2012) versus CLogP values describing the population of marketed against CLogP of CNS (vertical lines) and non-CNS (horizontal lines) drugs. There is a window between 2.5 and 4 CLogP for most marketed drugs.

In order to establish relevant structural activity relationships, it is important to evaluate how the structural changes proposed to improve the metabolic rate of lead structures – addition of fluorine at the active site of the molecule – could affect the permeability of the compound. Even though CLogP provides a prediction of how structural changes affect lipophilicity, it is necessary to actually determine the *in vitro* membrane transport rate of prospect compounds. Future studies will evaluate the GI track and BBB transport rates for the compounds in this study using in-house membrane transport assay in the Doll’s Lab.

Intrinsic Clearance Category

In **Table 4**, intrinsic clearance classifications were defined as “low” or “high” and their respective parameters were described for each biological species – human, dog,

monkey, rat, and mouse. For human models, *in vitro* intrinsic clearance – in units of $\mu\text{L}/\text{min}/\text{mg}$ protein – is low with a threshold of 8.6 and it is high with a threshold of 47. As shown in **Table 6**, intrinsic clearance of Amide-H (RD 53) and Urea-M (RD 89) are above the threshold of 47 $\mu\text{L}/\text{min}/\text{mg}$ protein, indicating that they are classified as high *in vitro* human intrinsic clearances. Although Urea-H (RD 38) does not fall above the threshold, it is above the median between low and high classification of intrinsic clearances, indicating that its *in vitro* human intrinsic clearance is potentially high. On the other hand, fluorinated compounds Amide-F (RD 78) and Urea-F (RD 86) have *in vitro* intrinsic clearances that are below the median, which indicates that they classify as medium to low *in vitro* intrinsic clearances using human liver microsomes.

In vitro intrinsic clearances for our fluorinated compounds, which fall between these thresholds, are further evidence that the structural changes made to the lead structures represent an improvement of the pharmacokinetic property of metabolic stability.

Marketed Drugs

To compare our compounds to some marketed drugs, the *in vitro* metabolic data has been collected for some marketed drugs such as midazolam, felodipine, propranolol, and nitredipine. The *in vitro* half-lives for these marketed drugs (Patten, 2009) are displayed in **Figure 60** alongside with the *in vitro* half-lives for our non-fluorinated compounds, Urea-H (RD 38) and Amide-H (RD 53), and our fluorinated compounds, Amide-F (RD 78) and Urea-F (RD 86). The methyl compound is also shown in **Figure 60**.

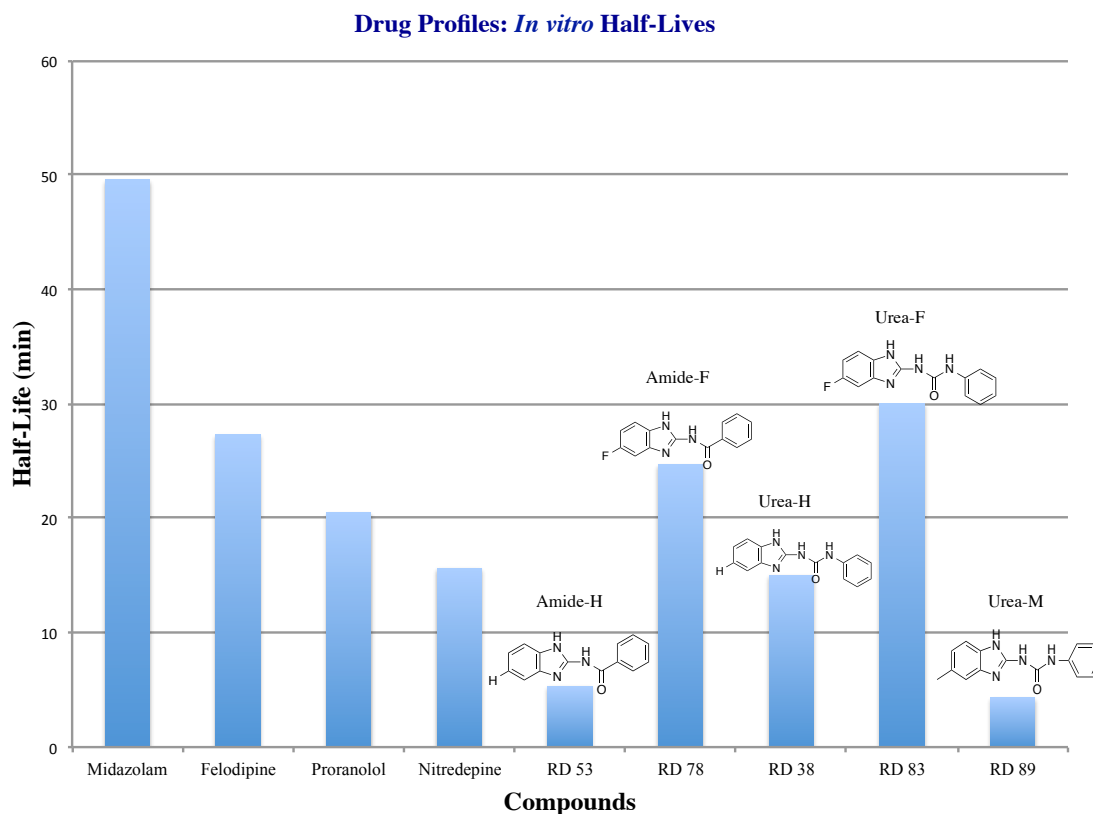


Figure 60. Comparison of *in vitro* half-lives for marketed drugs and RD compounds.

As shown in **Figure 60**, the RD compounds corresponding to the lead structures found in our laboratory – Urea-H (RD 38) and Amide-H (RD 53) – have *in vitro* metabolic rates that are faster than those of marketed drugs. For the fluorinated compounds Amide-F (RD 78) and Urea-F (RD 86), a clear improvement is observed, as these compounds' metabolic rates resemble more closely those of marketed drugs. To further test our hypothesis that cytochrome p450 shows high affinity for electron-rich systems, the metabolic rate for Urea-M (RD 89) was evaluated. The resulting rate for Urea-M (RD 89) is much faster than those of marketed drugs, indicating that addition of the electron-donating group to the structure metabolically activates the compound

towards hydroxylation by cytochrome p450. The goal of synthesizing more metabolically stable compounds to better match the metabolic rates to those of marketed drugs has been successfully achieved by addition of fluorine to the benzimidazole portion of the studied compounds.

CONCLUSION

As part of the drug discovery process is to optimize lead structures for potency, selectivity, and drug-like properties, it is important to establish structural activity relationships to succeed in the design of an overall effective drug. Regarding metabolic stability, it has been shown that structural changes affect phase I metabolism by cytochrome P450 in the liver metabolism, specifically impacting metabolic rate and the number of hydroxyl groups added. In this sense, electron-withdrawing groups like fluorine improved metabolic stability of compounds by lowering the *in vitro* intrinsic clearance. On the other hand, electron-donating groups such as methyl as substituents resulted in less metabolically stable compounds with higher *in vitro* intrinsic clearance. Furthermore, addition of the electron-withdrawing group, methyl, cause an increase in the number of hydroxylations that the compound undergoes.

The principles and techniques here can be applied to any drug discovery project as it sets an outline to the design of compounds around a biological target.

This study provided a better understanding of the metabolic fate of benzimidazole class of compounds and how to manipulate metabolic rates by performing structural changes. The knowledge acquired in this thesis regarding metabolic profiles, and the principles that lead to more metabolically stable compounds will be applied in the design of future anti-cancer compounds.

Future Considerations

To fully understand the metabolic profile of a drug, the specific cytochrome P450 isozyme responsible for the hydroxylation of the compound should be identified. This is important to determine possible drug-drug interactions. As a possible consideration to determine the specific isozymes involved in the liver metabolism of each of the fluorinated compounds, the microsomal assay can be performed in the same fashion but adding different known CYP inhibitors to the incubation tube. Inhibitors described in **Table 3** are commercially available or easily synthesized. If a change in the metabolic rate is observed upon the addition of an inhibitor, then we would be able to determine the isozymes responsible for the hydroxylation of the compound.

Furthermore, the metabolites identified for Amide-F (RD 78) and Urea-F (RD 86) can be synthesized to analyze their biological activity and toxicity to determine if they have biological activity. It is important to understand the biological activity of metabolites, especially if these compounds will stay in the system for a certain period of time.

As part of building a library of compounds with improved metabolic stability, other substituents such as bromine and chlorine should be studied. Both chlorine and bromine are not as electronegative as fluorine; however, these are bigger atoms that could inhibit metabolism by steric reasons. In addition, substituents such as $-CF_3$ or two fluorine substituents on the aromatic ring in the benzimidazole portion of the compound would be interesting systems to analyze in terms of their effects in metabolic profiles.

An alternative route to study the metabolic fate of compounds that undergo hydroxylation by CYP is the use of TAML activator as catalysts that mimic cytochrome p450. This would allow the precise identification of the structure of all metabolites.

Finally, the p53 reactivation biological activity for all newly synthesized compounds still has to be determined using biological assays. This is important because the ultimate goal of drug discovery is to optimize for potency, selectivity, and drug-like properties.

BIBLIOGRAPHY

- Andriole V.T. *The Quinolones*. Academic Press, 1989.
- American Cancer Society. *Cancer Facts & Figures 2013*. **2013**. Atlanta, GA: American Cancer Society.
- Barker H. A., Smyth R. D., Weissbach H., Toohey J. I., Ladd J. N., Volcani B. E. *Journal of Biological Chemistry*. **1960**. 235: 480–488.
- Barter Z.E., Martin K.B., Beaune P.H., Boobis A.R., Carlile D.J., Edwards R.J., Houston J.B., Lake B.G., Lipscomb J.C., Pelkonen O.R., Tucker G.T., Rostami-Hodjegan A. *Current Drug Metabolism*. **2007**. 8:33-45
- Blackwell H., Frei R., Breitbach A., Lynn D. M., Broderick A. H. U. S. Patent Application # 20130136782. **2013**
- Brown-Swigart L., Martins C. P., Evan L. G. *Cell*. **2006**. 127: 1323–1334
- Bullock A.N., Fersht A.R. *Nature*. **2001**. 1: 68-76
- Bykov V., Selivanova G., Wiman K. *European Journal of Cancer*. **2003**. 39: 1828-1834.
- Center for Drug Evaluation and Research. *Clinical Chemistry and Clinical Toxicology Devices Panel Meeting*. **1997**. Maryland: U. S. Food and Drug Administration.
- Chen P., Chen Y., Bookstein R., Lee W. *Science*. **1990**. 250. 4987: 1576-580.
- Cui B, Yang Q, Guan H, Shi B, Hou P, Ji M. *The Journal of Clinical Endocrinology and Metabolism*. **2014**.
- Dasmahapatra B., Neustadt B. R., Demma M., Mallams A. K., Vaccaro H. A., Pachter J. A. U. S. Patent Application #7,790,474. **2010**
- Danielson P.B., *Current Drug Metabolism*. **2002**. 3: 561-597.
- Duarte F.J. *Tunable Laser Applications*. CRC: New York. **2009**. Chapters 5, 7, 8.
- Di L., Kerns E. H. *Drug-like Properties: Concepts, Structure Design and Methods*. Princeton, NJ: Academic Press, **2011**.
- Enger, E. Concepts in Biology (7th Edition). McGraw-Hill. p. 173.**
- Galetin A., Houston J. B. *J. Pharmacol. Exp. Ther.* **2006**. 318: 1220-1229
- Ghose A. K.; Crippen G. M. *J. Comput. Chem.* **2012**, 7, 565- 577
- Goh A.M., Coffill C.R., Lane D.P. *Journal of Pathology*. **2011**. 223: 116-126.
- Griffin, J.P. *The Textbook of Pharmaceutical Medicine (6th Ed.)*. New Jersey: BMJ Books. **2009**.
- Hoe K. K., Verma C. S., Lane D. P. *Nature Reviews*. **2014**. 13: 217-136.
- Joerger A., Ang H., Fersht A. *Proceedings of the National Academy of Sciences*. **2006**. 41: 15056-15061
- Kitayner M et al. *Nature*. **2010**, 17, 423- 430
- Knights K., Bryant B. *Pharmacology for Health Professionals*. **2002**. Amsterdam: Elsevier.
- Lambert J. et al. *Cancer Cell*. **2009**. 15:376-388.
- Liu J. O., Shim J. S., Chong C. R., Bhat S. World Patent # WO 2010/042163 A2. **2009**
- Mizuno N., Niwa T., Yotsumoto Y., Sugiyama Y. *Pharmacology Review*. **2003**. 55: 425-

461

- Nassar A.F., Kamel A. M., Clarimont C. *Drug Discovery Today*. **2004**. 9:1020-1028
Pharmacokinetics. (2006). In *Mosby's Dictionary of Medicine, Nursing & Health Professions*. Philadelphia, PA: Elsevier Health Sciences. Retrieved October 16, 2015
- Patten C. *BD Biosciences*. **2009**
- Ruiz-Garcia A., Bermejo M., Moss A., Casabo V. G. *J. Pharm. Sci.* **2008**. 97: 654-690.
- Sneider W. *Drug Discovery: A History*. Hoboken, NJ: Wiley, **2005**.
- Subotic S., Wyler S., Bachmann A. *European Urology Supplements* **2012**. 11: 60–65.
- Takimoto R., Wang W., Dicker D., Rastinejad F., Lyssikatos J., El-Deiry W. *Cancer Biology and Therapy*. **2002**. 1: 47-55
- Turpeinen M., Uusitalo J., Jalonen J., Pelkonen O. *Eur. J. Pharm. Sci.* **2005**. 24: 123-132.
- Voet D., Voet J. G. *Biochemistry (3rd edition)*. Wiley. **2004**. p: 1309.
- Volgestein B., Lane D., Levine A. J., *Nature*. **2000**. 408: 307-310
- Wang, J., Urban L., Bojanic D. *Expert Opin. Drug Metab. Tox.* **2007**. 3: 641
- Wang W., Takimoto R., Rastinejad F., El-Deiry W.S. *Mol. Cell. Biol.* **2003**. 23:2171–2181.
- Walker M. G., Page C. P., Hoffman B. F., Curtis M. *Integrated Pharmacology (3rd ed.)*. **2006**. St. Louis: Mosby
- Weiss B., Hait W.N. *Ann. Rev. Pharmacol. Toxicol.* **1977**. 17:441-477.
- Wima, K. *Oncogene*. **2010**. 29: 4245-4252.
- Woosley R.L., Utrecht J.P., Sweetman B.J., , Oates J.A. *Drug Metab Dispos.* **1984**. 12:77-81.